Article

SOURCE DATA TRANSPARENT PROCESS

EMBO reports

Hypoxia causes pancreatic β-cell dysfunction and impairs insulin secretion by activating the transcriptional repressor BHLHE40

Tomonori Tsuyama[1], Yoshifumi Sato[2,*], Tatsuya Yoshizawa[2], Takaaki Matsuoka[3] & Kazuya Yamagata[1,2,**]

Abstract

Hypoxia can occur in pancreatic β-cells in type 2 diabetes. Although hypoxia exerts deleterious effects on β-cell function, the associated mechanisms are largely unknown. Here, we show that the transcriptional repressor basic helix–loop–helix family member e40 (BHLHE40) is highly induced in hypoxic mouse and human β-cells and suppresses insulin secretion. Conversely, BHLHE40 deficiency in hypoxic MIN6 cells or β-cells of *ob/ob* mice reverses defects in insulin secretion. Mechanistically, BHLHE40 represses the expression of *Mafa*, encoding the transcription factor musculoaponeurotic fibrosarcoma oncogene family A (MAFA), by attenuating the binding of pancreas/duodenum homeobox protein 1 (PDX1) to its enhancer region. Impaired insulin secretion in hypoxic β-cells was recovered by MAFA re-expression. Collectively, our work identifies BHLHE40 as a key hypoxia-induced transcriptional repressor in β-cells that inhibit insulin secretion by suppressing MAFA expression.

Keywords BHLHE40; hypoxia; insulin secretion; pancreatic β-cells; transcriptional repressor
Subject Category Molecular Biology of Disease
DOI 10.15252/embr.202256227 | Received 4 October 2022 | Revised 28 May 2023 | Accepted 4 June 2023 | Published online 21 June 2023
EMBO Reports (2023) 24: e56227

Introduction

Glucose metabolism is regulated by crosstalk between pancreatic β-cells and insulin-sensitive tissues. In case of insulin resistance, β-cells increase insulin secretion to maintain normal glucose tolerance. However, when β-cells are incapable of this task, plasma concentrations of glucose increase. Prolonged exposure to hyperglycaemia has deleterious effects on β-cell function through various mechanisms, including oxidative stress, endoplasmic reticulum (ER) stress, and inflammation and contributes to the development and progression of type 2 diabetes (Prentki & Nolan, 2006; Kahn *et al*, 2014; Hudish *et al*, 2019). Because β-cells are highly dependent on oxidative phosphorylation for adenosine triphosphate (ATP) production and insulin secretion, high-glucose conditions generate relative hypoxia in β-cells because these cells consume large amounts of oxygen (Sato *et al*, 2011; Bensellam *et al*, 2012, 2018; Ilegems *et al*, 2022). Importantly, hypoxia was shown to occur *in vivo* in islets in animal models of type 2 diabetes (Sato *et al*, 2011; Bensellam *et al*, 2012; Zheng *et al*, 2012; Ilegems *et al*, 2022). Like oxidative and ER stress, hypoxia leads to β-cell dysfunction and loss of β-cells, supporting the idea that hypoxia is another mechanism leading to β-cell failure in type 2 diabetes (Kitamura, 2013; Sato *et al*, 2014; Gerber & Rutter, 2017; Catrina & Zheng, 2021).

Hypoxia-inducible factor (HIF), a heterodimeric transcription factor consisting of an oxygen-sensitive HIF-α subunit and a constitutively expressed HIF-1β subunit, plays critical roles in the cellular responses to hypoxia (Gunton, 2020; Lee *et al*, 2020). HIF induces the expression of a number of genes necessary for adaptation to hypoxia, including those involved in glycolysis, erythropoiesis, and angiogenesis. However, hyperactivation of HIF in β-cells by von Hippel–Lindau deletion impairs insulin secretion by switching glucose metabolism from aerobic oxidative phosphorylation to anaerobic glycolysis (Zehetner *et al*, 2008; Cantley *et al*, 2009; Puri *et al*, 2009), suggesting that unregulated overactivation of HIF may cause β-cell dysfunction (Gunton, 2020; Catrina & Zheng, 2021). Besides gene induction, transcriptional repression of genes also occurs in response to hypoxia and was found to involve several transcription repressors, such as RE1 silencing transcription factor (REST), BTB and CNC homology 1 (BACH1), zinc finger E-box binding homeobox 1 (ZEB1), and inhibitor of DNA binding 2 (ID2; Cavadas *et al*, 2017). Previously, we reported that hypoxia causes the downregulation of a number of β-cell genes involved in insulin secretion in mouse islets and MIN6 β-cells (Sato *et al*, 2014). However, the mechanisms of hypoxia-induced transcriptional repression

1 Center for Metabolic Regulation of Healthy Aging (CMHA), Faculty of Life Sciences, Kumamoto University, Kumamoto, Japan
2 Department of Medical Biochemistry, Faculty of Life Sciences, Kumamoto University, Kumamoto, Japan
3 First Department of Internal Medicine, Wakayama Medical University, Wakayama, Japan
*Corresponding author. Tel: +81 96 373 5070; E-mail: ysato413@kumamoto-u.ac.jp
**Corresponding author. Tel: +81 96 373 5068; E-mail: k-yamaga@kumamoto-u.ac.jp

© 2023 The Authors

in β-cells and the contribution of gene repression to β-cell dysfunction are largely unknown.

In the present study, we identified the transcriptional repressor basic helix–loop–helix family member e40 (BHLHE40) as being highly induced in β-cells under hypoxic conditions and found that it inhibits glucose-stimulated insulin secretion by suppressing the transcription of *Mafa*, which encodes musculoaponeurotic fibrosarcoma oncogene family A (MAFA), a transcription factor that plays critical roles in insulin secretion. We also showed that BHLHE40 deficiency reversed decreased insulin secretion by hypoxic β-cells *in vitro* and *in vivo*. Our findings present a new scenario in which hypoxia impairs β-cell function through activation of the transcriptional repressor BHLHE40.

Results

Global gene expression in hypoxic β-cells and islets

To assess the impact of hypoxia on the global gene expression of β-cells, we first performed RNA sequencing (RNA-seq) on both mouse and human islets cultured under normal and low oxygen conditions. We previously reported that hypoxic responses occur at 5–7% oxygen tension in MIN6 cells and mouse islets and that 3% hypoxia for 24 h markedly increases MIN6 cell death (Sato *et al*, 2011, 2014). On the other hand, in human islets, a hypoxic response (induction of *SLC2A1* expression) was induced by exposure to 2% but not 5% oxygen tension (Fig EV1A) without apparent cell death. Therefore, for the hypoxic experiments, we used 5% oxygen in MIN6 cells and mouse islets and 2% oxygen in human islets. Approximately 5% of expressed mRNAs were significantly downregulated at least 1.5-fold in hypoxic compared with nonhypoxic islets (mouse, 20 vs. 5%, respectively; human, 20 vs. 2%, respectively; Fig EV1B). Consistent with our previous findings (Sato *et al*, 2014), under hypoxic conditions the expression of a number of β-cell genes with important roles in insulin secretion was decreased in islets (Fig 1A). Gene set enrichment analysis (GSEA) revealed that two hallmark gene sets (pancreas beta cells and oxidative phosphorylation) were significantly downregulated in both mouse and human islets in hypoxia and one hallmark gene set (hypoxia) was significantly upregulated (Figs 1B and EV1C). We hypothesized that transcriptional repressors are involved in the suppression of β-cell genes under hypoxic conditions. To identify the hypoxia-sensitive repressors in β-cells, we compared the RNA-seq–based data of hypoxia-induced genes in mouse islets, human islets, and MIN6 cells and found that 25 genes were elevated (Fig 1C). By analyzing the gene ontology of these genes, we discovered that activating transcription factor 3 (ATF3) and BHLHE40 are associated with transcriptional repression (Fig 1C). In addition, BHLHE41, REST, BACH1, ID1, ID2, ZEB1/ZEB2, and SNAI1 were reported elsewhere to function as hypoxia-induced transcriptional repressors (Cavadas *et al*, 2017). Among all these repressor genes, in our study, *Bhlhe40* mRNA was the most significantly increased in hypoxic mouse islets, human islets, and MIN6 cells (Fig 1D–F). Hypoxia-induced upregulation of *BHLHE40* was also detected in human islets from an independent donor (donor 2; Fig EV1D). BHLHE40 (also referred to as DEC1/SHARP2/STRA13) is a member of the basic helix–loop–helix (bHLH) family and functions primarily as a transcriptional repressor by binding to DNA at class B E-box motifs (St-Pierre *et al*, 2002). It plays pivotal roles in many biological processes, including cellular differentiation, cell growth, growth arrest, circadian rhythm, immunological response, and hypoxia, but its biological function in β-cells is unknown. Accordingly, we focused on the role of BHLHE40 in hypoxic β-cells.

Regulation of *Bhlhe40* expression in hypoxic β-cells and islets

BHLHE40 was expressed ubiquitously in adult mouse tissues, including pancreatic islets and MIN6 cells (Figs 2A and EV2A). Hypoxia rapidly increased the expression of *Bhlhe40* mRNA, that is, within 3 h, but a marked upregulation of BHLHE40 protein was noted at 12 h and this upregulation persisted at 24 h in MIN6 cells (Figs 2B and EV2B). Increased BHLHE40 expression in hypoxia was also detected in mouse islets (Figs 2C and EV2C).

Hypoxia induces oxidative and ER stress and activation of AMP-activated protein kinase (AMPK; Zheng *et al*, 2012; Görlach *et al*, 2015; Sato *et al*, 2017). However, in our study, oxidative stress (caused by treatment with H_2O_2), ER stress (caused by treatment with thapsigargin or tunicamycin), and AMPK activation (caused by treatment with metformin) did not increase expression of *Bhlhe40* mRNA in MIN6 cells (Fig 2D–F), suggesting that these processes are not involved in the induction of *Bhlhe40*. Previous studies showed that HIF-1 is involved in hypoxia-induced *Bhlhe40* expression (Miyazaki *et al*, 2002; Yun *et al*, 2002). Consistent with this finding, hypoxia-induced *Bhlhe40* mRNA expression was partially inhibited by the suppression of HIF-1β (Figs 2G and EV2D), indicating that hypoxia-induced *Bhlhe40* expression is partially HIF dependent in β-cells. We and others demonstrated that hypoxia occurs in islets in animal models of type 2 diabetes (Sato *et al*, 2011; Bensellam *et al*, 2012; Zheng *et al*, 2012). Consistent with this finding, levels of *Bhlhe40* mRNA and BHLHE40 were significantly elevated (2.3-fold and 4.5-fold, respectively) in islets of *ob/ob* mice (Fig 2H and I). Upregulation of BHLHE40 was detected also in islets of *db/db* mice (Figs 2J and EV2E). Intracellular localization of BHLHE40 varies by cells (Ivanova *et al*, 2005). Immunohistochemical analysis revealed strong BHLHE40 immunoreactivity in the cytoplasm of islets in *ob/ob* mice, but BHLHE40 staining was clearly detected also in the nucleus of islets (Fig 2K). The nuclear localization of BHLHE40 supports its function as a transcriptional repressor.

BHLHE40 controls insulin secretion in β-cells

To explore the role of BHLHE40 in β-cells, we generated *Bhlhe40* knockdown (KD) MIN6 cells. *Bhlhe40* deletion efficiency was 73.5% in MIN6 cells (Fig EV3A). Although BHLHE40 is reported to be involved in cell cycle and apoptosis regulation (Sato *et al*, 2016), hypoxia-induced growth inhibition (Fig EV3B) and cell death (Fig EV3C and D) were not restored in *Bhlhe40* KD MIN6 cells. Next, we investigated the impact of *Bhlhe40* KD on glucose-stimulated insulin secretion. As described previously (Sato *et al*, 2014), insulin secretion by high glucose was significantly decreased under hypoxic conditions without affecting insulin content (Figs 3A and EV3E). Of note, *Bhlhe40* KD significantly restored hypoxia-related decreased insulin secretion (Fig 3A), and conversely, *Bhlhe40* overexpression significantly attenuated insulin secretion without affecting the insulin content (Figs 3B and EV3F and G). These results indicate that

 © 2023 The Authors

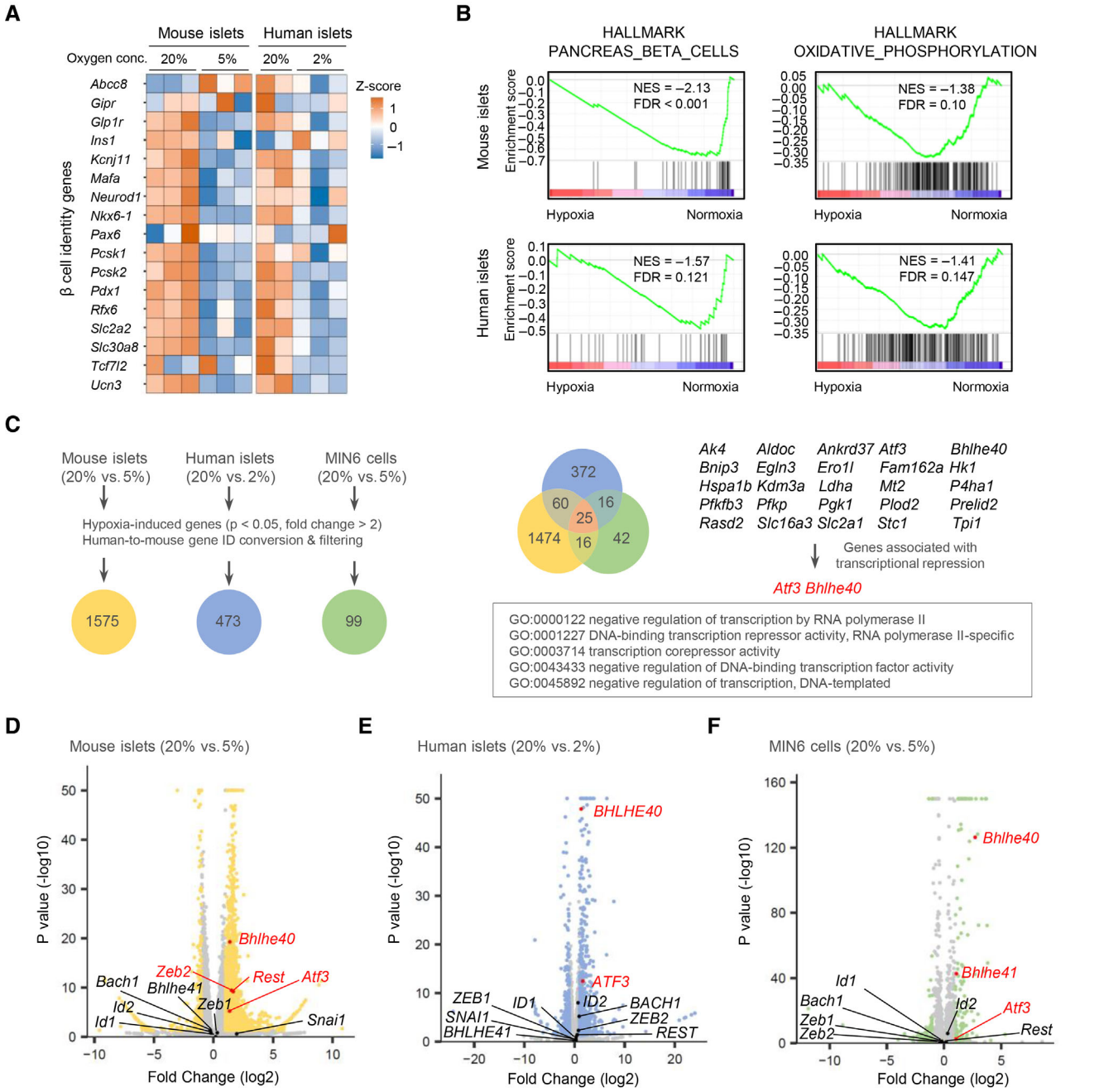

Figure 1. Global gene expression in hypoxic β-cells and islets.

A Heatmap of β-cell genes in mouse islets (20% vs. 5% O_2 for 24 h; n = 3 mice/group) and human islets (20% [n = 2 biological replicates from donor 1 sample] or 2% [n = 3 biological replicates from donor 1 sample] O_2 for 24 h).

B Gene set enrichment analysis of mouse islets (20% vs. 5% O_2 for 24 h; n = 3 mice/group) and human islets (20% [n = 2 biological replicates from donor 1 sample] or 2% [n = 3 biological replicates from donor 1 sample] O_2 for 24 h).

C RNA-seq data of hypoxia-induced genes in mouse islets (20% vs. 5% O_2 for 24 h; n = 3 mice/group), human islets (20% [n = 2 biological replicates from donor 1 sample] vs. 2% [n = 3 biological replicates from donor 1 sample] O_2 for 24 h), and MIN6 cells (20% vs. 5% O_2 for 6 h; n = 3 biological replicates). The Venn diagram shows the coordinated elevation of 25 genes, two of which (*Atf3* and *Bhlhe40*) are associated with transcriptional repression.

D–F Volcano plots showing RNA-seq data in mouse islets (20% vs. 5% O_2 for 24 h; n = 3 mice/group; D), human islets (20% [n = 2 biological replicates from donor 1 sample] vs. 2% [n = 3 biological replicates from donor 1 sample] O_2 for 24 h; E), and MIN6 cells (20% vs. 5% O_2 for 6 h; n = 3 biological replicates; F). *Atf3*, *Bhlhe40*, and other reported hypoxia-inducible transcriptional repressor genes (Cavadas *et al*, 2017) are shown (red, significantly upregulated genes).

BHLHE40 is involved in suppressing the glucose-stimulated insulin secretion. Glucose-stimulated insulin secretion occurs after the generation of ATP through the metabolism of glucose. The increase of the ATP/ADP ratio leads to the closure of ATP-sensitive K^+ channels, membrane depolarization, an increase of cytosolic $[Ca^{2+}]_i$ via activation of voltage-dependent Ca^{2+} channels, and eventually the

© 2023 The Authors

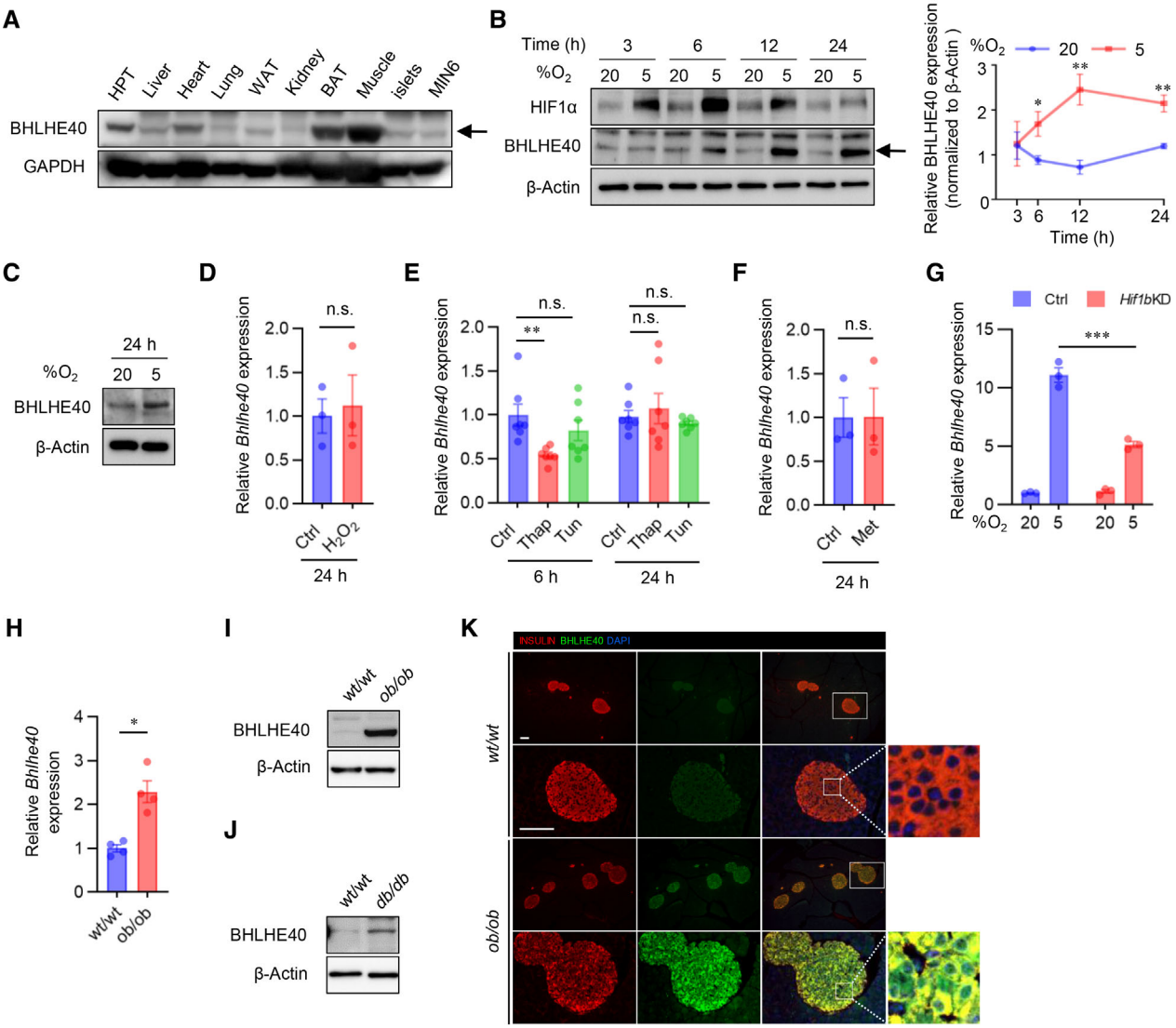

Figure 2. BHLHE40 expression and its regulation in hypoxic β-cells and islets.

A–C Western blots of BHLHE40 expression across tissues (A), BHLHE40 expression in MIN6 cells cultured under 20 or 5% O_2 for the indicated time (B) and the quantification of B (n = 3 biological replicates), and BHLHE40 expression in mouse islets cultured under 20 or 5% O_2 for 24 h (C).

D–F The effect of oxidative stress, endoplasmic reticulum stress, and energy stress on BHLHE40 expression. qRT–PCR analysis of *Bhlhe40* in MIN6 cells incubated with 10 μM H_2O_2 (n = 3 biological replicates; D), 2 μM thapsigargin (Thap) or 5 μg/ml tunicamycin (Tun) (n = 7 biological replicates; E), or 2 mM metformin (Met) for 24 h (n = 3 biological replicates; F).

G The effect of short-hairpin RNA-mediated *Hif1β* knockdown (KD) on BHLHE40 expression in MIN6 cells cultured under 20 or 5% O_2 for 24 h (n = 3 biological replicates).

H–K BHLHE40 expression in islets from diabetic mice. BHLHE40 expression was analyzed in *ob/ob* mouse islets by qRT–PCR (n = 4 biological replicates; H) and Western blotting (I) and in *db/db* mouse islets by Western blotting (J). Subcellular localization of BHLHE40 in *ob/ob* mice islets by immunohistochemical analysis (K).

Data information: Data are mean ± SEM; *P < 0.05, **P < 0.01, and ***P < 0.001 by unpaired two-tailed Student's t-test. Glyceraldehyde-3-phosphate dehydrogenase (GAPDH) or β-actin was used as a loading control. Scale bar, 100 μm. HPT—hypothalamus; Ctrl—control; n.s.—not significant.
Source data are available online for this figure.

exocytosis of insulin-containing secretory granules (Rorsman & Renström, 2003).

High K^+-induced membrane depolarization evokes Ca^{2+}-dependent insulin exocytosis from β-cells. We next investigated the role of BHLHE40 on KCl-stimulated insulin secretion. As in the case of glucose, a significant decrease in KCl-stimulated insulin secretion was detected in hypoxic MIN6 cells but not in hypoxic *Bhlhe40* KD MIN6 cells (Fig 3C). KCl produced a significantly smaller insulin secretion in MIN6 cells overexpressing *Bhlhe40* than in control MIN6 cells (Fig 3D). The observation that KCl induced an equivalent increase of $[Ca^{2+}]_i$ levels in both cells overexpressing *Bhlhe40* and control cells (Figs 3E and EV3H) suggests that BHLHE40 affects steps after $[Ca^{2+}]_i$ elevation. Next, we further explored the role of BHLHE40 on exocytosis by transfecting MIN6 cells with a human

 © 2023 The Authors

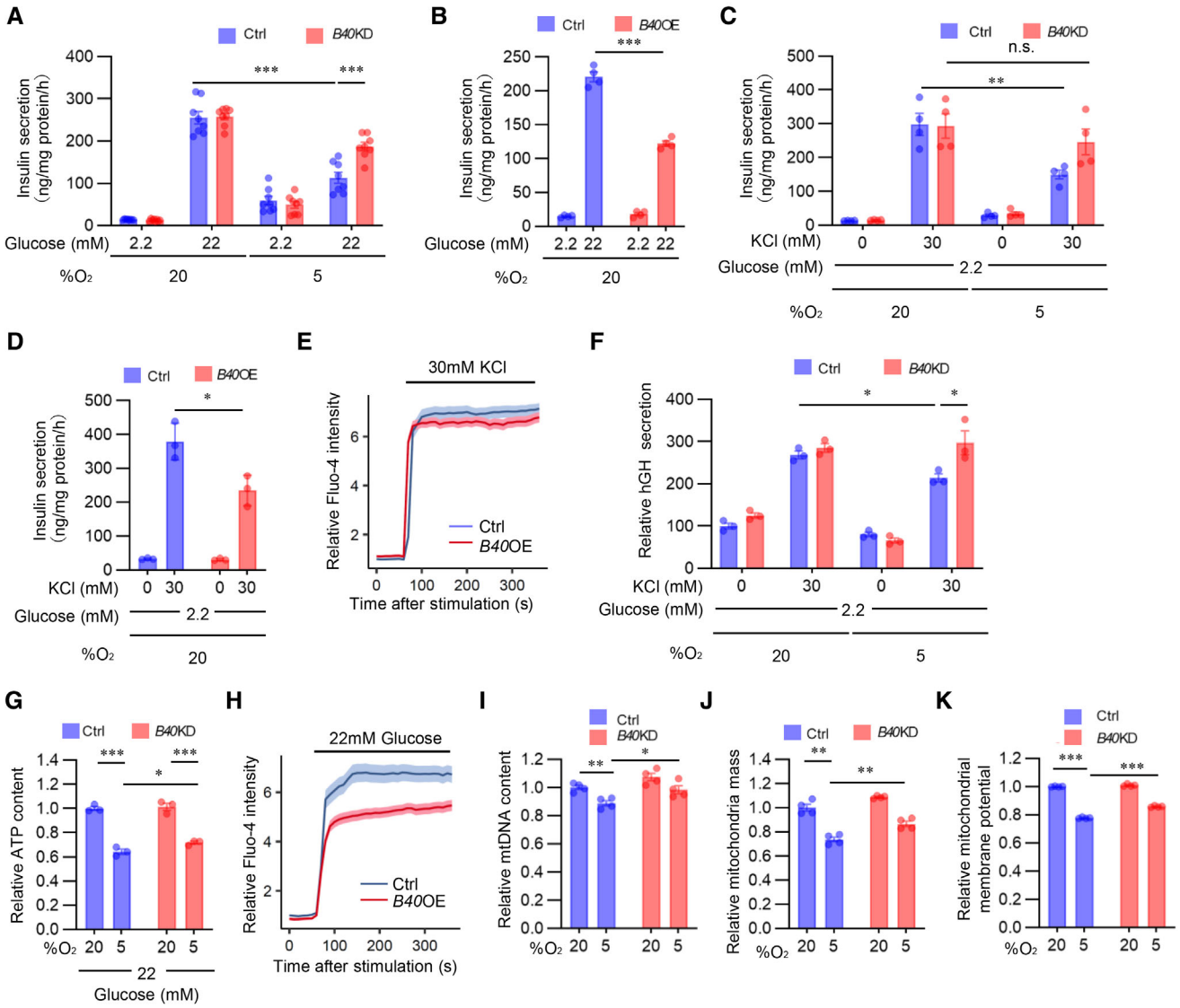

Figure 3. BHLHE40 controls insulin secretion in β-cells.

A Glucose-stimulated insulin secretion in MIN6 cells expressing short-hairpin RNA against a nontargeting Ctrl or *Bhlhe40* knockdown (*B40* KD) were cultured under 20 or 5% O_2 for 24 h (n = 8 biological replicates).

B Glucose-stimulated insulin secretion in MIN6 cells infected with retroviruses generated with pMx-Ctrl (Ctrl) or pMx-*Bhlhe40* (*B40* OE; n = 4 biological replicates).

C KCl-stimulated insulin secretion in Ctrl and *B40* KD MIN6 cells cultured under 20 or 5% O_2 for 24 h (n = 4 biological replicates).

D KCl-stimulated insulin secretion in Ctrl and *B40* OE MIN6 cells (n = 3 biological replicates).

E Calcium influx stimulated by 30 mM KCl in Ctrl and *B40* OE MIN6 cells (n = 70 cells from n = 3 biological replicates).

F hGH secretion after stimulation by 2.2 mM glucose or 2.2 mM glucose plus 30 mM KCl in Ctrl and *B40* KD MIN6 cells cultured under 20 or 5% O_2 for 24 h (n = 3 biological replicates).

G Cellular ATP content in Ctrl and *B40* KD MIN6 cells cultured under 20 or 5% O_2 for 24 h (n = 3 biological replicates).

H Calcium influx stimulated by 22 mM glucose in Ctrl and *B40* OE MIN6 cells (n = 70 cells from n = 3 biological replicates).

I–K Mitochondrial DNA (mtDNA) content (n = 4 biological replicates; I), mitochondrial mass (n = 4 biological replicates; J), and mitochondrial membrane potential (n = 4 biological replicates; K) in Ctrl and *B40* KD MIN6 cells cultured under 20 or 5% O_2 for 24 h.

Data information: Data are mean ± SEM; *P < 0.05, **P < 0.01, and ***P < 0.001 by unpaired two-tailed Student's t-test. Ctrl—control; n.s.—not significant. Source data are available online for this figure.

growth factor (hGH) expression vector. In transfected cells, hGH is targeted to insulin-containing secretory granules, and hGH release can be used to monitor exocytosis from the cells (Coppola *et al*, 1999; Fukui *et al*, 2005). As shown in Fig 3F, KCl-induced hGH secretion was significantly decreased under hypoxic conditions, and the decrease was almost completely reversed by *Bhlhe40* KD. These results emphasize the role of BHLHE40 in exocytosis in MIN6 cells.

To investigate the possibility that BHLHE40 affects multiple steps during glucose-stimulated insulin secretion, we next examined

© 2023 The Authors

glucose uptake in *Bhlhe40* KD and control MIN6 cells. Uptake of 2-NBDG, a fluorescent derivative of glucose, was decreased by hypoxia, but *Bhlhe40* KD did not affect 2-NBDG uptake in MIN6 cells (Fig EV3I), indicating that BHLHE40 does not affect glucose uptake. In line with our previous study (Sato *et al*, 2014), ATP levels in MIN6 cells were decreased under hypoxic conditions, and the decrease of ATP levels was significantly restored by *Bhlhe40* KD (Fig 3G). In addition, glucose-stimulated $[Ca^{2+}]_i$ levels were significantly attenuated by *Bhlhe40* overexpression (Figs 3H and EV3J). These results indicate that BHLHE40 suppresses glucose-stimulated ATP generation and the increase of $[Ca^{2+}]_i$ levels in MIN6 cells. Because mitochondria play important roles in ATP generation, we next investigated the impact of BHLHE40 on mitochondrial homeostasis. As shown in Fig 3I and J, the decreased mitochondrial DNA content and mass under hypoxic conditions were significantly recovered by *Bhlhe40* KD in MIN6 cells. Hypoxia significantly decreased the mitochondrial membrane potential, as measured with the voltage-sensitive mitochondrial dye MitoTracker Red (Fig 3K). Of note, BHLHE40 suppression recovered the loss of mitochondrial membrane potential in hypoxic MIN6 cells. These results strongly suggest that BHLHE40 suppresses mitochondrial biogenesis and function. Taken together, our results show that BHLHE40 affects at least two different steps, that is, ATP generation and exocytosis, during insulin secretion.

BHLHE40 suppresses *Mafa* expression in β-cells

To further understand how BHLHE40 regulates insulin secretion, we performed RNA-seq analysis in control MIN6 cells and MIN6 cells overexpressing *Bhlhe40*. Compared with control MIN6 cells, MIN6 cells overexpressing *Bhlhe40* showed 2,630 differentially expressed genes (1,288 downregulated and 1,342 upregulated; adjusted $P < 0.01$; Fig 4A). Gene ontology analysis revealed that the downregulated genes included transcription genes with critical roles during insulin secretion, including *Mafa*, *Nkx2-2*, *Ppargc1a*, *Vdr*, *Nkx6-1*, and *Neurod1* (Figs 4A and EV4A). Quantitative real-time polymerase chain reaction (qRT–PCR) in independent samples confirmed the significant downregulation of *Mafa*, *Nkx2-2*, *Ppargc1a*, and *Vdr* expression by *Bhlhe40* overexpression (Fig 4B). To validate that BHLHE40 functions as a repressor of these genes, we next examined their expression in *Bhlhe40* KD MIN6 cells under hypoxic conditions. Hypoxia significantly decreased *Mafa*, *Ppargc1a*, *Vdr*, and *Nkx6-1* mRNA, but the downregulation of *Mafa* was completely restored by KD of *Bhlhe40* (Fig 4C). At the protein level, the suppression of MAFA by BHLHE40 and restoration of hypoxia-induced downregulation of MAFA by BHLHE40 deficiency were also detected (Fig EV4B and C). MAFA regulates genes required for insulin exocytosis, including *Stxbp1* (encoding MUNC18-1), *Napa* (encoding N-ethylmaleimide-sensitive factor attachment protein), *Syt7* (encoding synaptotagmin 7), and *Stx1a* (encoding syntaxin1A; Nagamatsu *et al*, 1999; Ohara-Imaizumi *et al*, 2007; Oh *et al*, 2012; Hang *et al*, 2014; Dolai *et al*, 2016; Cataldo *et al*, 2022). Under hypoxic conditions, *Bhlhe40* KD also significantly restored the downregulation of *Stxbp1*, *Napa*, *Syt7*, and *Stx1a* (Fig 4D). Moreover, adeno-associated virus (AAV)-mediated overexpression of *Mafa* significantly increased the expression of these genes in MIN6 cells under hypoxic conditions (Fig EV4D and E). MAFA plays a critical role in both glucose- and KCl-stimulated insulin secretion (Zhang *et al*, 2005; Hang *et al*, 2014). Overexpression of *Mafa* did not alter the insulin content of hypoxic MIN6 cells (Fig EV4F). However, the glucose- and KCl-related decrease in insulin secretion (adjusted by insulin content) in hypoxic conditions was significantly restored by overexpression of *Mafa* (Fig 4E and F). ATP generation in MIN6 cells was not affected by *Mafa* overexpression (Fig EV4G). These results indicate that BHLHE40 suppresses insulin secretion, at least in part, by reducing the expression of MAFA in β-cells.

Peroxisome proliferator-activated receptor-γ coactivator 1-α (PGC-1α), which is encoded by *Ppargc1a*, regulates mitochondrial biogenesis and oxidative phosphorylation (Puigserver & Spiegelman, 2003). Previous studies revealed that BHLHE40 acts as a transcriptional repressor of *Ppargc1a* (Chung *et al*, 2015; LaGory *et al*, 2015). Consistent with this finding, *Ppargc1a* expression was significantly downregulated by *Bhlhe40* overexpression in MIN6 cells, and the hypoxia-induced downregulation of *Ppargc1a* was recovered by KD of *Bhlhe40* (Fig 4B and C). The mitochondrial respiratory subunits NDUFB8 and SDHB and the mitochondrial import receptor subunit TOM20 are known targets of PGC-1α (Kelly & Scarpulla, 2004; Scarpulla, 2008). The protein levels of NDUFB8, SDHB, and TOM20 were decreased by hypoxia, but the decrease was significantly reversed by *Bhlhe40* KD (Fig 4G). PGC-1α also

Figure 4. BHLHE40 suppresses *Mafa* expression in β-cells.

A MA plot of RNA-seq data in Ctrl and *B40* OE MIN6 cells. Differentially expressed genes (DEGs; adjusted *P*-value < 0.01) are shown in blue, and others in gray. DEGs functioning as β-cell transcription factors are shown in red ($n = 3$ biological replicates).

B, C Expression of DEGs shown in (A) was confirmed by qRT–PCR in Ctrl and *B40* OE MIN6 cells ($n = 3$ biological replicates; B) or Ctrl and *B40* KD MIN6 cells cultured under 20 or 5% O_2 for 24 h ($n = 3$ biological replicates; C).

D qRT–PCR of MAFA target genes in Ctrl and *B40* KD MIN6 cells cultured under 20 or 5% O_2 for 24 h ($n = 3$ biological replicates).

E Glucose-stimulated insulin secretion in MIN6 cells infected with AAV-GFP (Ctrl) or AAV-*Mafa* cultured under 20 or 5% O_2 for 24 h ($n = 8$ biological replicates). Insulin secretion was corrected for insulin content.

F KCl-stimulated insulin secretion in Ctrl and AAV-*Mafa* MIN6 cells cultured under 20 or 5% O_2 for 24 h ($n = 8$ biological replicates). Insulin secretion was corrected for insulin content.

G Western blot of oxidative phosphorylation complex proteins and TOM20 protein in Ctrl and *B40* KD MIN6 cells cultured under 20 or 5% O_2 for 24 h, and quantification of the band intensities ($n = 3$ biological replicates).

H, I qRT–PCR analysis of *Tfam* expression in Ctrl and *B40* OE MIN6 cells ($n = 3$ biological replicates; H) and in Ctrl and *B40* KD MIN6 cells cultured under 20 or 5% O_2 for 24 h ($n = 3$ biological replicates; I).

Data information: Data are mean ± SEM; *$P < 0.05$, **$P < 0.01$, and ***$P < 0.001$ by unpaired two-tailed Student's *t*-test. β-actin was used as a loading control. Ctrl—control.
Source data are available online for this figure.

 © 2023 The Authors

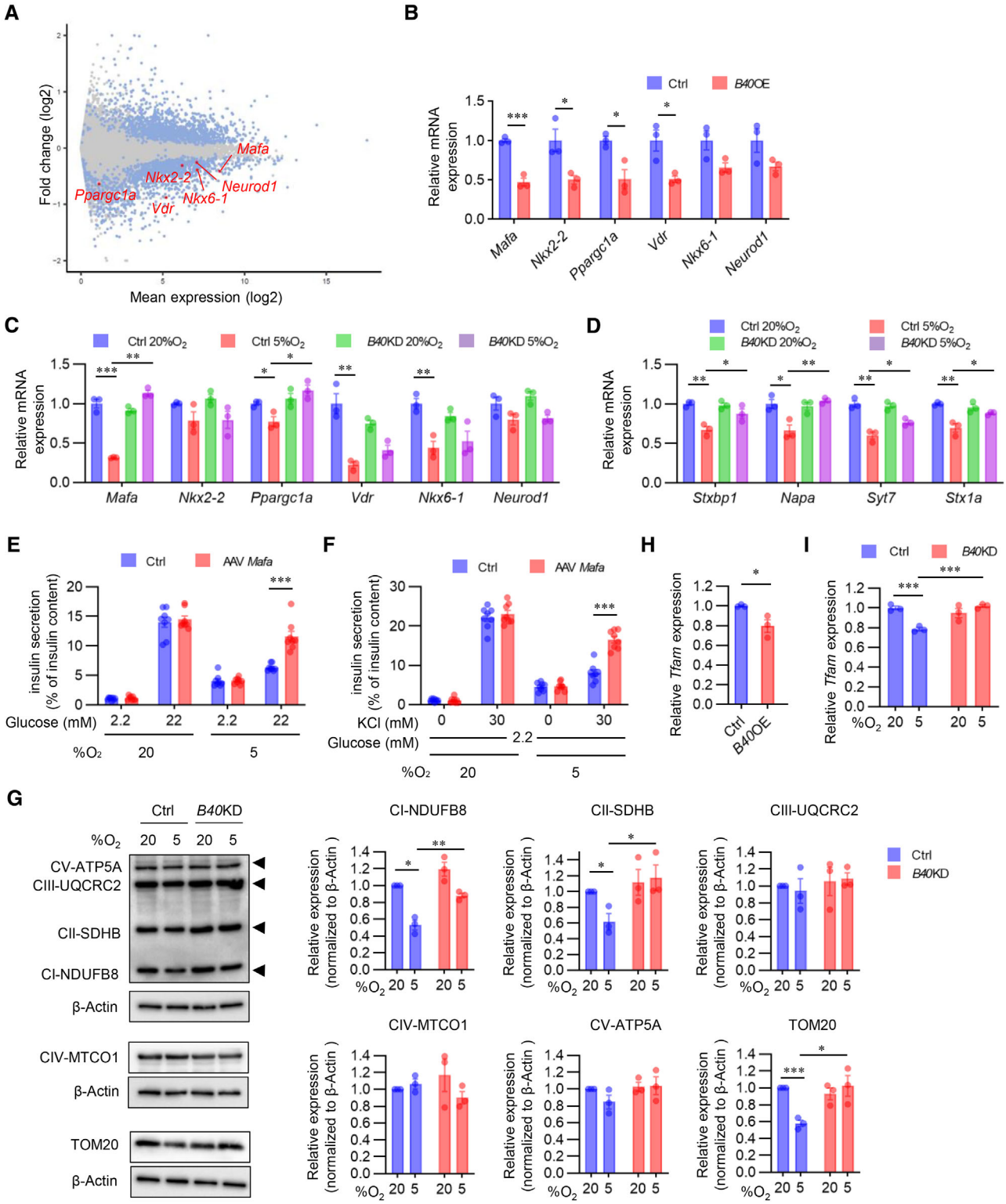

Figure 4.

induces the expression of mitochondrial transcription factor A (TFAM) (Puigserver & Spiegelman, 2003). *Tfam* expression was significantly downregulated by *Bhlhe40* overexpression, and the hypoxia-induced downregulation of *Tfam* was recovered by KD of *Bhlhe40* in MIN6 cells (Fig 4H and I). These results indicate that *Ppargc1a* is another target gene of BHLHE40 in MIN6 cells. In these experimental conditions, *Bhlhe40* KD did not affect the expression of *Nkx2-2*, *Vdr*, *Nkx6-1*, or *Neurod1* mRNAs (Fig 4C).

© 2023 The Authors

BHLHE40 controls *Mafa* expression via two E-box sites in the enhancer region

To further explore the mechanism by which BHLHE40 suppresses *Mafa* expression in β-cells, we performed a reporter gene assay with a reporter plasmid. We included the mouse *Mafa* enhancer/promoter region (−10,427 to +22 bp to transcriptional start site) because it shows maximum *Mafa* promoter activity in β-cells (Raum *et al*, 2006; Yamamoto *et al*, 2013). *Mafa* reporter gene activity was significantly decreased under hypoxic conditions, but the reduction was abolished by *Bhlhe40* KD (Fig 5A). BHLHE40 binds to E-box sequence (5′-CANNTG-3′) to suppress its target genes. Screening of the JASPAR database (Mathelier *et al*, 2016) revealed four E-box sites (A, −9,909/−9,899; B, −8,705/−8,695; C, −6,987/−6,976; and D, −4949/4938, relative score > 0.9) within the −10,427/+22 region (Fig 5B). Overexpression of *Bhlhe40* suppressed the activity of the reporter gene in MIN6 cells, but mutation of the A or C site in the reporter gene abolished the reduction of transcriptional activity by BHLHE40 (Fig 5C). Consistent with this finding, the suppression of the reporter gene activity by hypoxia also was attenuated by mutation of these two sites (Fig 5D). Furthermore, chromatin immunoprecipitation (ChIP) assay revealed enhanced binding of BHLHE40 to A and C sites in MIN6 cells under hypoxic conditions (Fig 5E). These results indicate that BHLHE40 suppresses *Mafa* expression by binding to the A or C site. BHLHE40 is reported to repress the transcription of the target genes by recruiting histone deacetylase (HDAC; Sun & Taneja, 2000; Chung *et al*, 2015). However, treatment with trichostatin A (TSA), an HDAC inhibitor, failed to affect the reduced reporter gene activity in hypoxic MIN6 cells (Fig 5F).

The transcription factor pancreas/duodenum homeobox protein 1 (PDX1) was reported to regulate *Mafa* expression in β-cells by binding to the enhancer region (−8,152 to −7,780 relative to the transcription start site; Raum *et al*, 2006, 2010). Therefore, we investigated whether BHLHE40 represses *Mafa* expression by inhibiting PDX1 binding (Fig 5G). Intriguingly, the ChIP assay revealed that BHLHE40 significantly reduced PDX1 binding to the *Mafa* gene in MIN6 cells (Fig 5H). The reduction of PDX1 binding to the *Mafa* gene was also detected under hypoxic conditions (Fig 5G, I, and J). These results suggest that BHLHE40 controls *Mafa* expression, at least in part, by affecting the binding of PDX1.

Deficiency of BHLHE40 improves hyperglycaemia in *ob/ob* mice

To evaluate the role of BHLHE40 *in vivo*, we generated β-cell–specific *Bhlhe40* knockout (*βB40*KO) mice by crossing *Pdx1*-Cre mice (Skarnes *et al*, 2011) with floxed *Bhlhe40* (*Bhlhe40*^{fl}) mice (Fig EV5A). The *Bhlhe40* deletion efficiency in the *βB40*KO islets was 74.1% (Fig EV5B). Body weight (Fig EV5C) and nonfasting blood glucose concentration (Fig EV5D) were similar in *βB40*KO and *Bhlhe40*$^{fl/fl}$ mice, and the intraperitoneal glucose tolerance test also showed no differences in blood glucose levels among *Pdx1*-Cre, *Bhlhe40*$^{fl/fl}$, and *βB40*KO mice (Fig 6A).

BHLHE40 negatively regulates insulin secretion, and BHLHE40 expression was markedly upregulated in *ob/ob* pancreatic islets (Fig 2I). We then investigated the effects of β-cell–specific BHLHE40 deficiency in *ob/ob* mice (*βB40*KO:*ob/ob* mice). In these mice, BHLHE40 deficiency in β-cells had no effect on obesity (Fig 6B), insulin sensitivity (Fig EV5E), or nonfasting glucose concentrations (Fig EV5F). However, the mice displayed better glucose tolerance than control *Bhlhe40*$^{fl/fl}$:*ob/ob* (control:*ob/ob*) mice (Fig 6C and D). In agreement with the results obtained in MIN6 cells, glucose-stimulated insulin secretion was significantly increased in *βB40*KO:*ob/ob* mice (Fig 6E). The insulin content of control and *βB40*KO islets was similar (Fig EV5G). However, insulin secretion by high glucose (Fig 6F) and KCl (Fig 6G) was also increased in *βB40*KO islets under hypoxic conditions. We measured the ATP content with 2.2 and 22 mM glucose under hypoxic conditions and found that ATP levels were significantly increased in *βB40*KO islets compared with control islets (Fig 6H). There was no significant difference in the ratio of β-cell area to whole pancreas area between *βB40*KO:*ob/ob* and control:*ob/ob* mice (Fig 6I and J), but stronger nuclear immunostaining of MAFA was detected in *βB40*KO:*ob/ob* mice (Fig 6K and L). Lastly, the increased expression of *Mafa*, *Stxbp1*, *Napa*, *Syt7*, *Stx1a*, *Ppargc1a*, and *Tfam* in *βB40*KO:*ob/ob* islets was confirmed by qRT–PCR (Fig 6M). Taken together, the results show that BHLHE40 deficiency improves glucose tolerance in *ob/ob* mice by enhancing insulin secretion.

Figure 5. BHLHE40 controls *Mafa* expression via two E-box sites in the enhancer region.

A Reporter gene analysis with luciferase plasmid infused with mouse MAFA promoter/enhancer (−10,427/+22 bp from transcription start site) in Ctrl and *B40* KD MIN6 cells cultured under 20 or 5% O_2 for 24 h (n = 4 biological replicates).

B BHLHE40-binding motif (left) and JASPAR results (right) are presented. JASPAR predicted four E-box sites for BHLHE40 binding on MAFA promoter/enhancer (relative score > 0.9, E-box sites are underlined).

C Luciferase reporter assay was performed with MIN6 cells transfected with BHLHE40 expression plasmids, pRL-SV40 plasmid, and pGL3-Mafa plasmids (wild-type [black] and E-box mutated [red] sites; n = 4 biological replicates).

D Luciferase reporter activity in MIN6 cells cultured under 20 or 5% O_2 for 24 h (n = 3 biological replicates).

E MIN6 cells were cultured in 20 or 5% O_2 for 24 h, and then the proteins were immuno-precipitated by IgG or anti-BHLHE40 specific antibody, after which qRT–PCR was performed for the indicated regions (n = 3 biological replicates).

F Luciferase reporter assay in MIN6 cells incubated with 0.1 μM TSA or vehicle for 24 h (n = 4 biological replicates).

G ChIP–qPCR scheme for checking PDX-1 binding to *Mafa* enhancer.

H–J Proteins sampled from Ctrl and *B40* OE MIN6 cells with FLAG-Pdx1 expression (H) or from MIN6 cells with FLAG-Pdx1 expression precultured under 20 or 5% O_2 for 24 h (I) were immuno-precipitated by IgG or anti-FLAG antibody, after which qRT–PCR was performed for the indicated regions (n = 9 biological replicates for H and n = 6 biological replicates for I). FLAG (PDX1) expression in (I) was confirmed by Western blotting (J).

Data information: Data are mean ± SEM; *P < 0.05 **P < 0.01, and ***P < 0.001 by unpaired two-tailed Student's t-test. Ctrl—control; n.s.—not significant.
Source data are available online for this figure.

 © 2023 The Authors

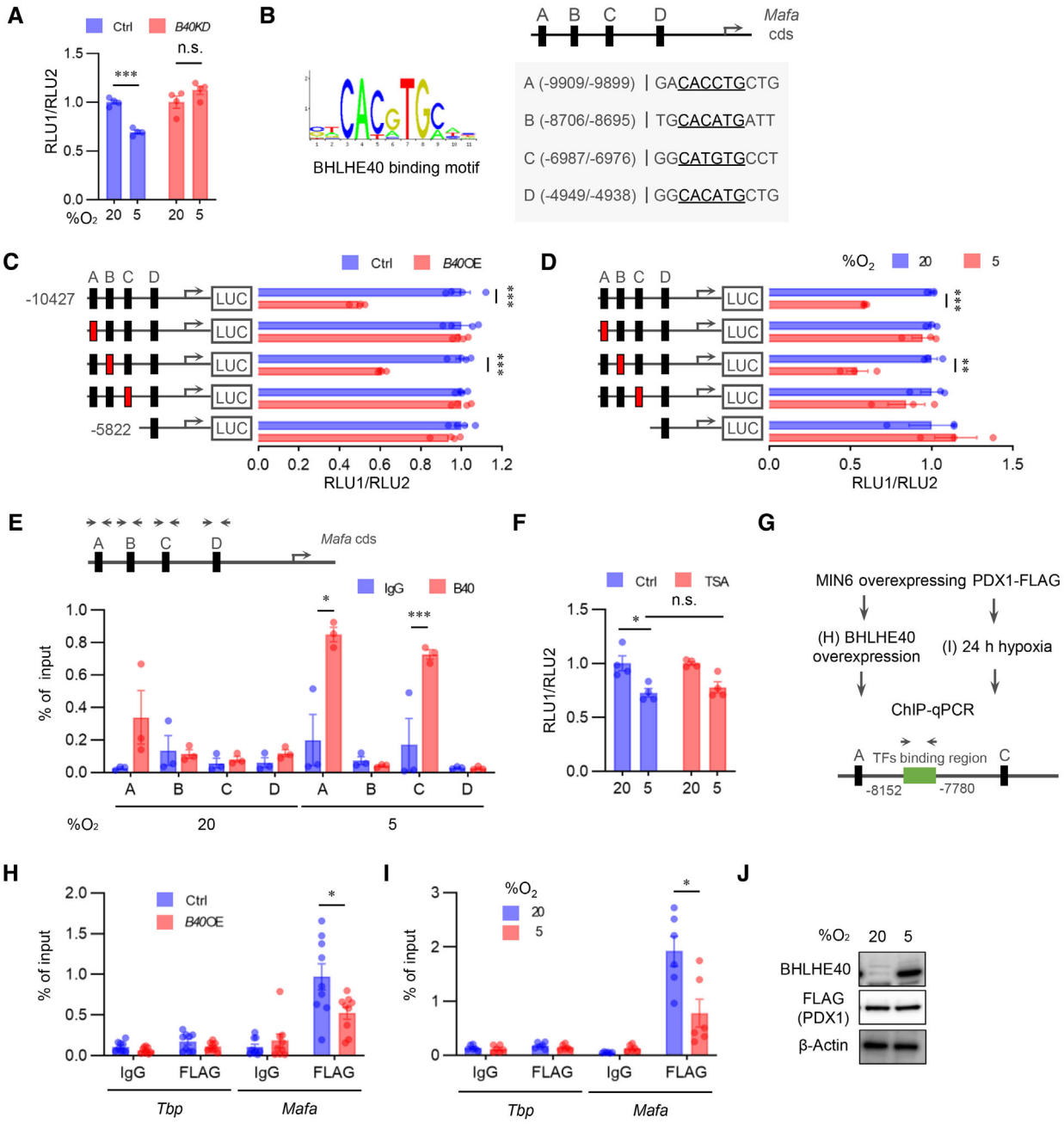

Figure 5.

Discussion

Adaptation to hypoxia involves three major responses: increased glycolysis to cope with ATP depletion, increased oxygen delivery, and inhibition of energy-demanding processes such as gene transcription (Cavadas *et al*, 2017). HIF transcriptional factors are known to play central roles in glycolytic ATP production and oxygen delivery, but the mechanisms underlying transcriptional repression in hypoxia are poorly understood. By screening hypoxia-induced genes in mouse and human islets and MIN6 cells, we showed that the transcriptional repressor BHLHE40 is highly induced in hypoxic β-cells. We also demonstrated that BHLHE40 negatively regulates insulin secretion by suppressing the transcription of *Mafa* (Fig 7).

In addition, we found that BHLHE40 suppresses the transcription of *Ppargc1a* and decreases ATP levels in β-cells. PGC-1α plays important roles in mitochondrial biogenesis and ATP production (Lin *et al*, 2005; Ling *et al*, 2008). Thus, it is plausible that the decreased expression of PGC-1α may be involved in the reduced ATP levels and impaired insulin secretion under hypoxic conditions. However, the impact of ATP generation due to BHLHE40 deficiency was relatively mild, and the glucose- and KCl-related insulin secretory profiles were similar both *in vitro* and *ex vivo* in the presence of genetic manipulations of *Bhlhe40*, suggesting a more prominent role

© 2023 The Authors

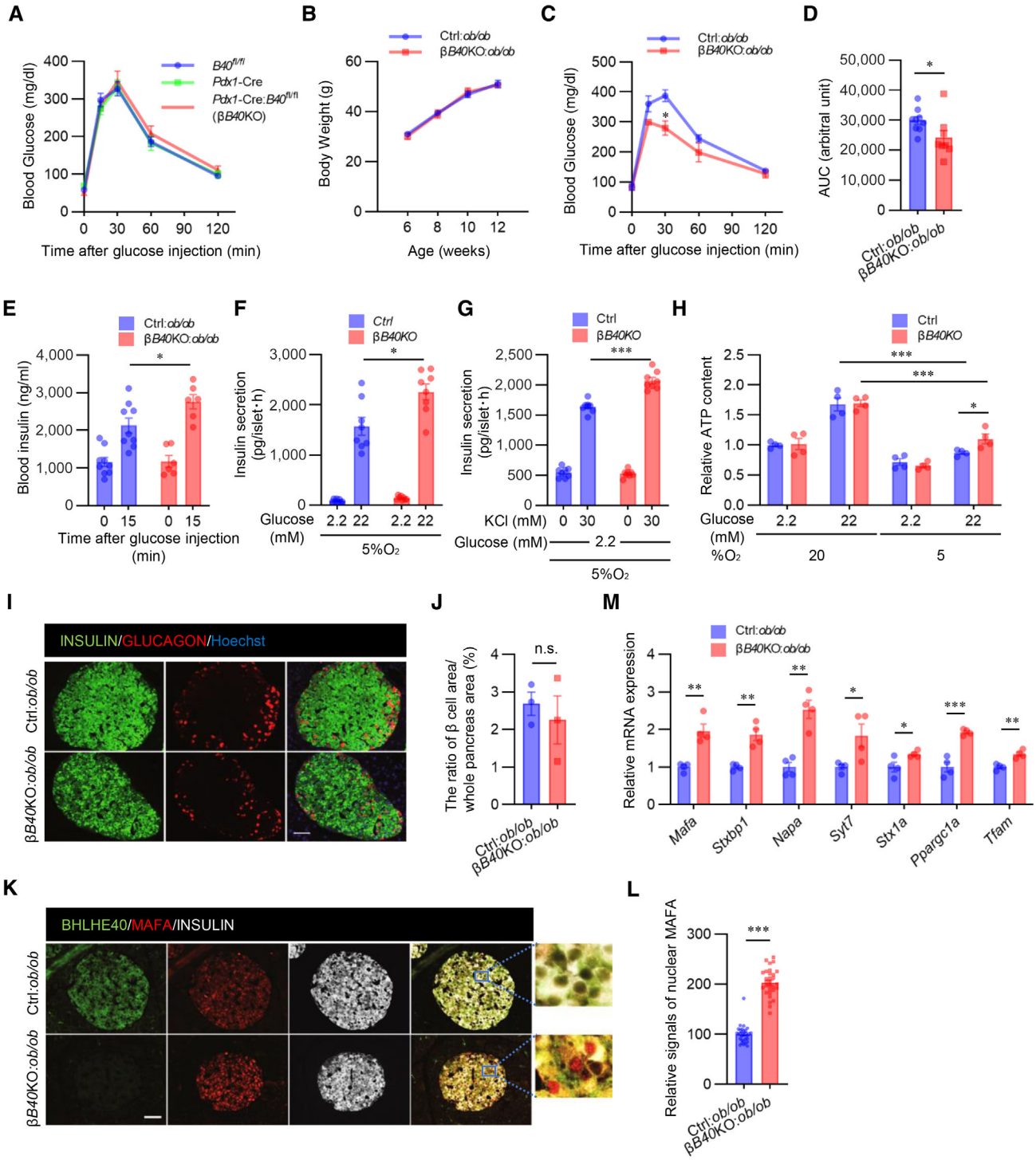

Figure 6.

of BHLHE40 in regulating exocytotic events. Further studies are necessary to evaluate the contribution of *Mafa* and *Ppargc1a* to a hypoxia-induced defect in insulin secretion.

BHLHE40 was previously reported to suppress the transcription of target genes by recruiting HDACs (Sun & Taneja, 2000; Chung *et al*, 2015). By contrast, we found that TSA treatment did not relieve the BHLHE40-mediated repression of *Mafa*, indicating that *Mafa* repression by BHLHE40 is independent of the recruitment of HDAC. On the other hand, we demonstrated that BHLHE40 inhibits the binding of PDX1 to the critical enhancer region of *Mafa*. Repressors are reported to regulate transcription by interacting with activator proteins (Gaston & Jayaraman, 2003). BHLHE40 might suppress *Mafa* transcription by interacting with PDX1. Alternatively, BHLHE40 might change DNA conformations by recruiting

 © 2023 The Authors

Figure 6. Deficiency of BHLHE40 improves hyperglycaemia in *ob/ob* mice.

A Glucose tolerance test of *Pdx1*-Cre (*Cre*), *Bhlhe40*$^{fl/fl}$ (*B40*$^{fl/fl}$), and *Pdx1*-Cre:*Bhlhe40*$^{fl/fl}$ (*Cre:B40*$^{fl/fl}$) mice (n = 7 mice, n = 12 mice, and n = 9 mice, respectively; 8–12 weeks old).

B Body weight of *Bhlhe40*$^{fl/fl}$ (Ctrl):*ob/ob* and *Pdx1*-Cre:*Bhlhe40*$^{fl/fl}$ (β*B40*KO):*ob/ob* mice (n = 9 mice and n = 6 mice, respectively).

C, D Glucose tolerance test of Ctrl:*ob/ob* and β*B40*KO:*ob/ob* mice (n = 9 mice and n = 8 mice, respectively; 6 weeks old) (C) and AUC (D).

E Glucose-stimulated insulin secretion in Ctrl:*ob/ob* and β*B40*KO:*ob/ob* mice (n = 9 mice and n = 6 mice, respectively; 8 weeks old).

F Glucose-stimulated insulin secretion in isolated islets from Ctrl and β*B40*KO mice after culture under 5% O_2 for 24 h (n = 8 biological replicates).

G KCl-stimulated insulin secretion in isolated islets from Ctrl and β*B40*KO mice after incubation with 5% O_2 for 24 h (n = 8 biological replicates).

H ATP content in isolated islets of Ctrl and β*B40*KO mice after incubation with 20% or 5% O_2 for 24 h (n = 4 biological replicates).

I, J Representative images of pancreatic islets stained for insulin and glucagon in Ctrl:*ob/ob* and β*B40*KO:*ob/ob* mice (12 weeks old) (I). The ratios of total islet area to whole pancreas area (%) are shown (n = 3 biological replicates; J).

K, L Representative images of pancreatic islets stained for insulin, MAFA, and BHLHE40 in Ctrl:*ob/ob* and β*B40*KO:*ob/ob* mice (12 weeks old) (K). Fluorescence intensities of nuclear and cytosolic MAFA in K were quantified (n = 30 cells; L).

M qRT–PCR of *Mafa* and its target genes in Ctrl:*ob/ob* and β*B40*KO:*ob/ob* mice (n = 4 mice).

Data information: Data are mean ± SEM; *P < 0.05 **P < 0.01, and ***P < 0.001 by unpaired two-tailed Student's t-test. Scale bar, 10 μm. Ctrl—control; n.s.—not significant.
Source data are available online for this figure.

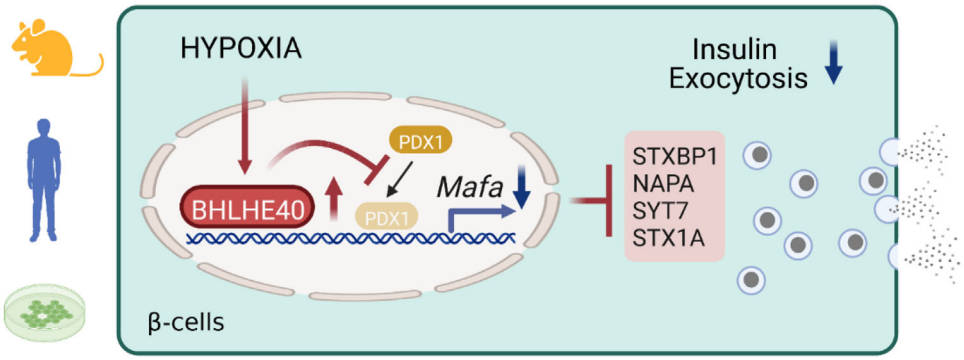

Figure 7. A proposed model for how hypoxia causes β-cell dysfunction

chromatin-remodeling factors. The family of large Maf proteins comprises MAFA, MAFB, and MAF (c-Maf). Intriguingly, recent studies demonstrated that BHLHE40 represses the expression of *Mafb* and *Maf* mRNAs in macrophages (Jarjour *et al*, 2019). Thus, BHLHE40 seems to be a common repressor of the large Maf family. Further studies are necessary to clarify the mechanism by which BHLHE40 suppresses these genes.

In the present study, we showed that approximately 5% of genes were downregulated in hypoxic islets. In addition to BHLHE40, we also found an increased expression of ATF3 in β-cells in hypoxia. Previously, ATF3 was reported to regulate the expression of genes related to glucose metabolism, inflammation, and apoptosis (Li *et al*, 2008; Zmuda *et al*, 2010a, 2010b; Ku & Cheng, 2020). Consistent with the findings (Li *et al*, 2008; Zmuda *et al*, 2010b), the suppression of the genes *Ins1*, *Ins2*, and *Irs2* by hypoxia was significantly reversed in *Atf3* KD MIN6 cells (Appendix Fig S1A and B). In addition, hypoxia-induced upregulation of the proinflammatory *Il1b* and proapoptotic *Noxa* genes and activation of caspase-3 were significantly suppressed by KD of *Atf3* in MIN6 cells (Appendix Fig S1C and D). Also, hypoxia-induced apoptosis was significantly decreased in *Atf3* KD MIN6 cells (Appendix Fig S1E). Thus, hypoxia might affect β-cell function and death through not only BHLHE40 but also other transcriptional factors, such as ATF3.

In diabetes, the β-cells are in a vicious cycle in which an impaired insulin response to glucose produces hyperglycemia, which stresses β-cell function and makes β-cells more inefficient, and reversal of hyperglycemia results in at least partial recovery of β-cell function (Turner *et al*, 1976; Prentki & Nolan, 2006). We showed that the suppression of BHLHE40 improves glucose tolerance in *ob/ob* mice by increasing insulin secretion. Thus, inhibition of BHLHE40 might be beneficial for preventing progressive β-cell dysfunction in type 2 diabetes. Further studies are necessary to deepen our understanding of BHLHE40 as a therapeutic target in type 2 diabetes.

Material and Methods

Mouse models

C57B6 wild-type (WT), *ob/ob*, and *db/db* mice were purchased from KBT Oriental Co., Ltd. (Saga, Japan). Mice carrying the Bhlhe40$^{tm1a(KOMP)Wtsi}$ allele (C57BL/6NTac-Bhlhe40tm1a(KOMP) Wtsi/WtsiPh, EM:09819) were obtained from the European Conditional Mouse Mutagenesis Program (EUCOMM) and crossed with *FLPe* mice (B6-Tg(CAG-FLPe)36, RBRC01834, RIKEN BRC, Ibaraki, Japan) to remove a LacZ reporter and a Neo cassette flanked by two Frt sites. To achieve a *Bhlhe40* deletion in β-cells, Bhlhe40$^{fl/fl}$ mice

© 2023 The Authors

were further crossed with *Pdx1*-Cre mice (gift from Dr. Douglas A. Melton). β-cell–specific Bhlhe40 knockout mice on *ob/ob* background were generated by crossing with Bhlhe40$^{fl/fl}$:*ob/+* mice and *Pdx1*-Cre:Bhlhe40$^{fl/fl}$:*ob/+* mice. Mice were housed under a 12-h light/dark cycle with free access to water and normal chow (CE-2; CLEA, Tokyo, Japan). Room temperature was maintained at 22 ± 1–2°C.

Human pancreatic islets

Human islets were commercially purchased from Prodo Laboratories (Irvine, CA). The cadaveric donors had no history of diabetes (donor 1: 32-year-old male; BMI, 25.1; HbA1c, 5.1%; donor 2: 54-year-old male; BMI, 21.6; HbA1c, 5.2%). Islets were cultured according to the Prodo Laboratories' instructions. Islets from donor 1 were used for RNA-seq and qRT–PCR, and islets from donor 2 were used for qRT–PCR.

Cell lines

MIN6 cells were gifts from Jun-ichi Miyazaki (Osaka University). They were maintained in Dulbecco's modified Eagle's medium (DMEM) supplemented with 10% (v/v) fetal bovine serum (FBS), 0.1% (v/v) penicillin/streptomycin (P/S), and 50 μM β-mercaptoethanol at 37°C in 5% CO_2, 95% air. For the hypoxic cell culture, a multi-gas incubator (APM-300; ASTEC, Fukuoka, Japan) was used. Retroviral packaging cell line Platinum-E (Plat-E; RV-101) cells were purchased from Cell Biolabs, Inc. (San Diego, CA). They were maintained in DMEM supplemented with 10% (v/v) FBS and 0.1% (v/v) P/S at 37°C in 5% CO_2, and 95% air. 293AAV cells were purchased from Cell Biolabs Inc. (AAV-100). They were maintained in DMEM with sodium pyruvate supplemented with 10% (v/v) FBS, 1× Glutamax, 1× Opti-MEM, and 0.1% (v/v) P/S at 37°C in 5% CO_2, 95% air.

Plasmids

The HA-tagged mouse *Bhlhe40* coding sequence was excised from a pCAGGS-DEC1 plasmid (RDB08473, Riken, Saitama, Japan; Nishiyama *et al*, 2012) and subcloned into pcDNA3.1 and pMXs-Puro Retroviral vector (RTV-012, Cell Biolabs, Inc.). For knockdown experiments, oligonucleotide encoding *Bhlhe40* short-hairpin RNA (shRNA; target sequence: 5′-GCACGTGAAAGCATTGACA-3′; Shen *et al*, 2014), *Atf3* shRNA (target sequence: 5′-GCAGAAAGAGTCAGAGAAACT-3′), and *Hif1β* shRNA (target sequence: 5′-GGACAGAGATCCAAGGTTT-3′) were cloned into the pSIREN-RetroQ expression vector (631526; Clontech Laboratories Inc., Mountain View, CA). The FLAG-tagged mouse *Pdx1* coding sequence was amplified by PCR and subcloned into a pMXs-Neo Retroviral vector (RTV-011, Cell Biolabs, Inc.). pGL3-basic-*Mafa* plasmid (−10427/+22 from transcription start site) was previously reported (Yamamoto *et al*, 2013). The pGL3-basic-*Mafa* plasmids with single deletion of the E-box site at −9,910/−9,899 (A; GAAAAATGCTG), −8,706/−8,695 (B; TGAAAATGATT), or −6,987/−6,976 (C; GGAAAATGCCT) were generated with a KOD-Plus Mutagenesis Kit (SMK-101, TOYOBO, Osaka, Japan). The truncated pGL3-basic-*Mafa* plasmid (−5,811/+22) was generated by BglII digestion and religation. The mouse *Mafa* coding sequence was amplified by PCR and subcloned into pAAV-MCS (VPK-410, Cell Biolabs. Inc.).

MIN6 cells stably overexpressing/silencing a target gene

To generate stable overexpression cell lines, retroviral vectors (pMx-Puro-HA-*Bhlhe40*, pMx-Puro Control, pMx-Neo FLAG-*Pdx1* or pMx-Neo Control plasmid) were transfected into Plat-E cells with JetPRIME transfection reagent (114-15, Polyplus, New York, NY), and MIN6 cells were infected with the respective retroviruses and selected by incubation with puromycin (5 μg/ml) for 2 days or G418 (500 μg/ml) for 4 weeks. For stable knockdown of *Bhlhe40*, pSIREN-RetroQ-*Bhlhe40* or pSIREN-RetroQ-control vector was transfected into Plat-E cells, and MIN6 cells were infected with the retroviruses and selected by incubation with puromycin (5 μg/ml) for 2 days.

AAV-*Mafa* preparation

293AAV cells were plated onto 10-cm dishes. At 80% confluency, cells were transfected with 2 μg/dish pAAV-DJ, 3 μg/dish pHelper, and either 2 μg/dish pAAV-green fluorescent protein (GFP) or pAAV-*Mafa* with JetPRIME transfection reagent. Three days after transfection, AAV-GFP and AAV-*Mafa* were purified with the AAV pro Extraction Solution Kit (6235, Takara, Shiga, Japan), and the titers were determined with a Quick Titer AAV Quantification Kit (VPK-145, Cell Biolabs, Inc.) according to the manufacturer's instructions.

Isolation of mouse islets

Mice were euthanized by cervical dislocation and subjected to bile duct cannulation and digestion of the pancreas with a mixture of collagenase P (11-249-002-001, Roche, Basel, Switzerland), hyaluronidase (H3506; Sigma-Aldrich, St. Louis, MO, USA), and protease inhibitor cocktail (Nacalai Tesque, Kyoto, Japan) for 25–30 min in a warm (37°C) water bath. Isolated islets were collected manually. Islets were maintained in RPMI-1640 supplemented with 10% (v/v) FBS, 0.1% (v/v) P/S, 50 μM β-mercaptoethanol, 10 mM HEPES, and 1 mM sodium pyruvate at 37°C in 5% CO_2, 95% air.

qRT–PCR

MIN6 cells were homogenized in Sepasol-RNA I reagent (09379-55, Nacalai Tesque), and RNA was manually isolated by phenol-chloroform extraction and ethanol precipitation. RNA from isolated islets was prepared with the RNeasy Micro Kit (74004, QIAGEN, Hilden, Germany) according to the manufacturer's instructions. cDNA was synthesized with a Prime Script RT Reagent Kit (RR047A, Takara Bio Inc., Shiga, Japan). qRT–PCR was performed with SYBR Premix Ex TaqII (RR820A, Takara Bio Inc.) in an ABI 7300 thermal cycler (Applied Biosystems, Foster City, CA) or a ViiA 7 Real-Time PCR System (Thermo Fisher Scientific, Waltham, MA). All data were normalized to *Actb* or *Tbp*. The primers for this study are listed in Appendix Table S1.

RNA-seq analysis

RNA was extracted with the RNeasy Micro Kit (74004, QIAGEN) according to the manufacturer's instructions. For Fig 1 samples, sequencing libraries were prepared with a NEBNext Ultra II

 © 2023 The Authors

Directional RNA Library Prep Kit (7765L, New England Biolabs, Ipswich, MA), and samples were sequenced on an Illumina NextSeq 500 platform in 76 bp single-end reads. For Fig 4 samples, sequencing libraries were prepared with a NEBNext Ultra II RNA Library Prep Kit (E7770, New England Biolabs) and samples were sequenced on an Illumina NovaSeq 6000 platform in 150 bp paired-end reads. For reanalysis of RNA-seq data of *db/db* mice islets (accession number: GSE 107489; John *et al*, 2018), raw RNA-seq data were downloaded from NCBI Sequence Read Archive and converted to the fastq format with SRA-Tools (v2.10.9). Reads were trimmed for universal Illumina adaptors with TrimGalore (v0.6.5) (https://www.bioinformatics.babraham.ac.uk/projects/trim_galore/) and then mapped to GENCODE 36 genome sequence (for human) or M25 genome sequence (for mouse) with HISAT2 (v2.2.1; Kim *et al*, 2019). Mapped reads were sorted and converted to a binary alignment/map format with SAMtools (v1.11; Li *et al*, 2009). Gene assembly and quantification were performed with Stringtie (v2.1.4; Pertea *et al*, 2015), and gene-level count matrixes were generated with Python script prepDE.py3 (http://ccb.jhu.edu/software/stringtie/dl/prepDE.py3). Differentially expressed genes (DEGs) were determined with DESeq2 (v1.28.0; Love *et al*, 2014). DEGs (adjusted *P*-value < 0.01) were used for gene ontology analysis with David (v6.8; Huang *et al*, 2009a,b).

Screening for hypoxia-induced genes associated with transcriptional repression

Hypoxia-induced genes were defined as genes with an adjusted *P*-value of less than 0.05 and a fold change (hypoxia/normoxia) greater than 2 in DESeq2 outputs. To identify hypoxia-induced genes that are commonly listed in mouse and human islets and MIN6 cells and are related to transcriptional repression, DESeq2 outputs in each group were processed as follows: For human islets, human-to-mouse Ensembl gene identifiers (IDs) conversion was carried out with Ensembl BioMart; and for MIN6 cells and mouse islets, only genes with mouse Ensembl gene IDs that can be mapped to those in human were selected. After this gene IDs conversion and gene filtering, overlapped genes were determined. Genes associated with transcriptional repression were manually selected out of the overlapped genes based on gene ontology annotations against each gene (obtained from Ensembl BioMart).

GSEA

Gene set enrichment analysis was performed with GSEA (v4.03; Subramanian *et al*, 2005) for "preranked" analyses, with the fold change between normoxia samples and hypoxia samples as the input. Mouse Ensembl IDs were converted to be compatible with the human annotations of the MSigDB gene lists by using a Mouse ENSEMBL Gene ID to Human Orthologs MSigDB.v7.4.chip.

Western blotting

Cells were lysed in RIPA buffer (50 mM Tris–HCl [pH 8.0], 150 mM NaCl, 0.1% sodium dodecyl sulfate [SDS], 1% NP-40, 5 mM EDTA, and 0.5% sodium deoxycholate) with a protease inhibitor cocktail. Total proteins were separated by SDS–polyacrylamide gel electrophoresis, transferred to polyvinylidene difluoride membranes (Immuno-P; Millipore, Bedford, MA), and then probed with the primary antibody. After incubation with the horseradish peroxidase (HRP)-conjugated secondary antibodies, the HRP signals were visualized by using Chemi-Lumi One Super (02230-30, Nacalai Tesque) and a ChemiDocTM Imaging System (Bio-Rad Laboratories, Hercules, CA) or a LAS-1000 imaging system (FUJIFILM Corporation, Tokyo, Japan). The primary antibodies used in this study were anti-β-actin antibody (M177-3, MBL), anti-BHLHB2 antibody (H00008553-M01, Abnova), anti-cleaved caspase-3 (9661, Cell Signaling Technology, Danvers, MA), anti-DYKDDDDK (FLAG) tag antibody (clone 1E6, 018-22381, Wako Pure Chemical Industries, Ltd., Osaka, Japan), anti-MafA antibody (A300-611A, Bethyl Laboratories, Montgomery, TX), anti-glyceraldehyde-3-phosphate dehydrogenase (GAPDH) antibody (2118, Cell Signaling Technology), anti-HIF1α antibody (NB100-479, Novus Biologicals, Centennial, CO), anti-HIF1β antibody (5537, Cell Signaling Technology), anti-TOM20 (11802-1-AP, Proteintech Group Inc., Rosemont, IL), and total OXPHOS rodent WB antibody cocktail (ab110413, Abcam, Cambridge, UK). Band intensities were quantified with Image Lab Software version 6.0 (Bio-Rad Laboratories).

Insulin secretion assay and insulin content in MIN6 cells

MIN6 cells were seeded in a 24-well plate. In Figs 3A and C, 4E and F, EV3E, and EV4F, cells were incubated in 20 or 5% O_2 for 24 h before assay. Cells were preconditioned in low-glucose (2.2 mM) Krebs-Ringer-bicarbonate HEPES (KRBH) buffer (120 mM NaCl, 4.7 mM KCl, 1.2 mM KH_2PO_4, 2.4 mM $CaCl_2$, 1.2 mM $MgCl_2$, 20 mM $NaHCO_3$, 10 mM HEPES, and 0.5% [v/v] BSA) for 1 h. Cells were washed once with low-glucose KRBH and incubated in low-glucose KRBH for 1 h, and the supernatant was collected. Then, cells were stimulated in high-glucose (22 mM) KRBH or low-glucose + KCl (30 mM) KRBH for 1 h, and the supernatant was collected. Next, cells were lysed in cell lysis buffer, and the protein concentration was measured with a Pierce BCA Protein Assay Kit (23225, Thermo Fisher Scientific, Waltham, MA) to normalize the insulin level. To measure insulin content, MIN6 cells were pelleted and resuspended in acid-ethanol (1.5% HCl in 70% EtOH), rotated overnight at 4°C and neutralized with 1 M Tris–HCl (pH 7.5; 1:1). The insulin concentration was determined with a mouse insulin enzyme-linked immunosorbent assay (ELISA; TMB) kit (AKRIN-011T; Shibayagi Co., Ltd., Gunma, Japan). A hypoxia chamber glove box (Creative Bio Station: CBS-120; ASTEC) was used to achieve continuous hypoxic conditions during the assay.

Insulin secretion assay and insulin content in mouse islets

The islets isolated from Ctrl and β*B40*KO mice were cultured in 5% O_2 for 24 h. Then, they were preincubated for 30 min in KRBH buffer containing 2.2 mM glucose. For glucose challenge, they were incubated in KRBH buffer containing 2.2 or 22 mM glucose for 30 min, and the supernatant was collected; and for KCl challenge, they were incubated in KRBH buffer containing 2.2 or 2.2 mM glucose plus 30 mM KCl for 30 min, and the supernatant was collected. To measure insulin content, isolated islets cells were pelleted and resuspended in acid-ethanol (1.5% HCl in 70% EtOH), rotated overnight at 4°C, and neutralized with 1 M Tris–HCl (pH 7.5; 1:1). The insulin concentration was determined with a mouse insulin ELISA (TMB) kit

© 2023 The Authors

(AKRIN-011T and AKRIN-011S; Shibayagi Co., Ltd.). A hypoxia chamber glove box (Creative Bio Station: CBS-120; ASTEC) was used to achieve continuous hypoxic conditions during the assay.

Cell proliferation assay

Before the assay, Ctrl or *Bhlhe40* KD MIN6 cells were seeded in a 96-well plate at 2×10^4 cells/well, incubated overnight, and transferred to 20 or 5% O_2. Cells were counted at 0, 24, 48, and 96 h with a Cell Counting Kit-8 (343-07623, Dojindo, Kumamoto, Japan), and the absorbance (450/655) was measured by an iMark microplate reader (Bio-Rad Laboratories).

Cell death assay

Before the assay, Ctrl or *Bhlhe40* KD MIN6 cells were transferred to and cultured in 20 or 5% O_2 for 24 h. The cells were incubated in PI and Annexin V solution according to the instructions in the Annexin V-Fluorescein Isothiocyanate (FITC) Apoptosis Detection Kit (K101-100; BioVision, Milpitas, CA). Then, flow cytometric analyses were performed with a FACSCalibur (BD Biosciences, Franklin Lakes, NJ) and FlowJo software (Tomy Digital Biology, Tokyo, Japan).

Calcium assay

Ctrl or *Bhlhe40* OE MIN6 cells were plated on glass-bottomed culture dishes (627871, Greiner Bio-One, Frickenhausen, Germany). The cells were preincubated with KRBH buffer for 45 min and then incubated with KRBH buffer containing 2.2 mM glucose, 2 μM Fluo4-AM (F311, Dojindo), 0.02% Pluronic F-127 (P2443, Sigma-Aldrich), 2.5 mM probenecid (162-26112, Wako Pure Chemical Industries, Ltd.), and Hochest 33258 (343-07961, Dojindo) for 30 min, after which the buffer was replaced with dye-free KRBH buffer. For KCl challenge, buffer was changed by hand aspirating it and an equal amount of KRBH buffer containing 2.2 mM glucose and 30 mM KCl was gently added to the dish using a micropipette. For glucose challenge, buffer was changed by hand aspirating it and adding an equal amount of KRBH buffer containing 22 mM glucose. Time-series images were acquired every 10 s with a fluorescent microscope (BZ-X700; Keyence, Osaka, Japan) and analyzed with Keyence software.

hGH secretion assay

Ctrl or *Bhlhe40* KD MIN6 were transfected with either pcDNA3-empty or pcDNA3-hGH. At 24 h after transfection, cells were transferred to and cultured in 20 or 5% O_2 for a further 24 h. Cells were preincubated in glucose-free KRBH for 15 min and then incubated in KRBH with or without KCl (30 mM) for 30 min, and the supernatant was collected. Cells were then lysed in cell lysis buffer, and the protein concentration was measured with a Pierce BCA Protein Assay Kit (23225, Thermo Fisher Scientific) to normalize the hGH level. The hGH concentration was measured with Human Growth Hormone ELISA kit (ab190811, Abcam, Cambridge, UK).

Glucose uptake assay

Before the assay, Ctrl or *Bhlhe40* KD MIN6 cells were transferred to and incubated in 20 or 5% O_2 for 24 h. Cells were preincubated in KRBH for 15 min and then incubated in KRBH containing 200 μM 2-NBDG (23002-v, Peptide Institute, Inc., Osaka, Japan) plus 22 mM glucose for 15 min, after which flow cytometric analyses were performed with FACSCalibur (BD Biosciences) and FlowJo software (Tomy Digital Biology).

Evaluation of mtDNA content

MIN6 were digested with 300 μg/ml proteinase K (Nacalai Tesque) in DNA lysis buffer (100 mM Tris–HCl pH 8.5, 5 mM EDTA, 0.2% SDS, 200 mM NaCl) at 55°C overnight with shaking, and DNA was then extracted with protein precipitation solution (Promega Corporation, Madison, WI) and phenol/chloroform. mtDNA content was evaluated by determining the ratio of mtDNA to nuclear DNA (nDNA). mtDNA was amplified by using primers specific for the mitochondrially encoded NADH dehydrogenase 1 (*mt-Nd1*) gene and normalized to nDNA by amplifying platelet/endothelial cell adhesion molecule 1 (*Pecam1*). The primer sequences are listed in Appendix Table S1.

Mitochondrial mass assay

Before the assay, Ctrl or *Bhlhe40* KD MIN6 cells were transferred to and incubated in 20 or 5% O_2 for 24 h. Then, cells were incubated in 2 nM nonyl acridine orange (A-1372, Invitrogen, Carlsbad, CA) for 15 min, after which flow cytometric analyses were performed with FACSCalibur (BD Biosciences) and FlowJo software (Tomy Digital Biology).

Mitochondrial membrane potential assay

Before the assay, Ctrl or *Bhlhe40* KD MIN6 cells were transferred to and incubated in 20 or 5% O_2 for 24 h. Then, cells were incubated in 25 nM MitoTracker Red (PA-3017, Lonza, Walkersville, MD) for 20 min, after which flow cytometric analyses were performed with FACSCalibur (BD Biosciences) and FlowJo software (Tomy Digital Biology).

Luciferase assay

MIN6 cells were transiently transfected with firefly luciferase plasmid (either pGL3-basic-MafA or its derivatives) and renilla luciferase plasmid (pRL-SV40) with jetPRIME transfection reagent (114-15, Polyplus). For *Bhlhe40* overexpression experiments, *Bhlhe40* expression plasmids (either pcDNA3.1-empty or pcDNA3.1-*Bhlhe40*) were additionally transfected. Forty-eight hours after transfection, cells were lysed and assayed with firefly luciferase and renilla luciferase substrates in the Dual-Luciferase Reporter Assay System (E1980, Promega). Firefly luciferase activity (RLU1) was normalized to renilla luciferase activity (RLU2). For hypoxia experiments, cells were transferred to 20 or 5% O_2 for 24 h before the luciferase activities were measured.

ChIP assay

MIN6 cells were fixed in 1% formaldehyde for 10 min at room temperature, and then the reaction was quenched by 150 mM glycine for 5 min. The fixed cells were incubated in 0.5% Nonidet P-40 lysis

 © 2023 The Authors

buffer for 15 min on ice, and the nuclei were pelleted and incubated in SDS lysis buffer (50 mM Tris–HCl [pH 8.0], 1% SDS, 10 mM EDTA). Chromatin was then sheared with a Bioruptor sonicator (C30010016, Diagenode, Seraing, Belgium) by 10 cycles of sonication at 30 s on and 30 s off. The sheared chromatin was diluted 5-fold in ChIP dilution buffer (50 mM Tris–HCl [pH 8.0], 167 mM NaCl, 1.1% Triton X-100, and 0.11% sodium deoxycholate) and then incubated in Dynabeads protein A (1001D, Invitrogen) and protein G (1003D, Invitrogen) for 1 h at 4°C. After removing the beads, the chromatin was incubated in 4 μg of anti-Bhlhe40 antibody (NB100-1800, Novus Biologicals), anti-DYKDDDDK (FLAG) tag antibody (clone 1E6, 018-22381, Wako Pure Chemical Industries, Ltd.), or control IgG (2729, Cell Signaling Technology) overnight at 4°C. The antibody-protein complexes were isolated by incubation with magnetic beads (Invitrogen Dynabeads protein A and protein G) for 6 h at 4°C. Then, samples were sequentially washed with low-salt RIPA buffer (50 mM Tris–HCl [pH 8.0], 150 mM NaCl, 1 mM EDTA, 0.1% SDS, 1% Triton X-100, and 0.1% sodium deoxycholate), high-salt RIPA buffer (50 mM Tris–HCl [pH 8.0], 500 mM NaCl, 1 mM EDTA, 0.1% SDS, 1% Triton X-100, and 0.1% sodium deoxycholate), LiCl wash buffer (10 mM Tris–HCL [pH 8.0], 250 mM LiCl, 1 mM EDTA, 0.5% Nonidet P-40, and 0.5% sodium deoxycholate), and Tris–EDTA buffer and finally eluted and reversely cross-linked in ChIP direct elution buffer (50 mM Tris–HCl [pH 8.0], 5 mM EDTA, and 0.5% SDS) overnight at 65°C. DNA was then extracted and collected by phenol-chloroform extraction and ethanol precipitation. DNA was amplified by qRT–PCR with SYBR Premix Ex Taq II (RR820A, Takara) in ABI 7300 thermal cycler (Applied Biosystems) or ViiA 7 Real-Time PCR System (Thermo Fisher Scientific) with the primers listed in Appendix Table S1.

Metabolic analysis of mice

Male 6- to 12-week-old mice were used for metabolic analysis. For the glucose tolerance test, mice were fasted overnight. After intraperitoneal glucose administration (2 g/kg for wild-type background, 1 g/kg for *ob/ob* background), blood glucose levels were measured at 0, 15, 30, 60, 90, and 120 min. For the insulin tolerance test, mice were fasted for 4 h. After intraperitoneal insulin administration (1 unit/kg for wild-type background, 3 units/kg for *ob/ob* background), blood glucose levels were measured at 0, 30, 60, 90, and 120 min. For the glucose-stimulated insulin secretion assay, mice were fasted overnight. After intraperitoneal administration of 3 g/kg glucose, blood samples were collected at 0 and 15 min. The plasma insulin level was determined with a mouse insulin ELISA (TMB) kit (AKRIN-011S; Shibayagi Co., Ltd.).

Immunohistochemistry and β-cell mass assessment

Pancreas tissues from mice were fixed with 10% (v/v) neutral buffered formalin (060–01667, Wako Pure Chemical Industries, Ltd.) for 16–18 h at 4°C. Fixed samples were embedded in paraffin, cut into 4-μm cross-sections, and mounted on MAS-coated slides (Matsunami Glass, Osaka, Japan). The deparaffinized sections were subjected to antigen retrieval (110°C, 20 min) with HistoVT One (L6F9587, Nacalai Tesque) and stained with the following primary antibodies: anti-insulin antibody (A0564, 1:400; Dako, Santa Clara, CA), anti-glucagon antibody (ab92517, 1:400; Abcam), anti-DEC1/BHLHE40 antibody (NB100-1800, 1:100; Novus Biologicals), and anti-MafA antibody (A300-611A, 1:100; Bethyl Laboratories). After reaction with fluorescent dye-conjugated secondary antibodies, fluorescent signals were captured with an all-in-one fluorescent microscope (BZ-X700; Keyence). The total islet area (μm^2) composed of insulin- and glucagon-stained cells was measured by Keyence software, and the ratio of the total islet area to the total pancreas area was calculated.

Statistical analyses

The significance of differences was assessed by unpaired two-sided Student's *t*-tests, unless stated otherwise. All data are presented as means ± SEM. No statistical analysis was used to predetermine the sample size.

Study approval

The handling and killing of mice were performed in compliance with the animal care guidelines of Kumamoto University. All animal experiments were conducted in accordance with the guidelines of the Institutional Animal Committee of Kumamoto University and were approved by the Kumamoto University Ethics Review Committee for Animal Experimentation (ID: A29-001, A 2019-048, A 2021-001). Human islet experiments were approved by the Ethical Committee of Kumamoto University Graduate School of Medical Sciences (No. 2389).

Data availability

The RNA-seq datasets generated in this study are available in the Gene Expression Omnibus repository and have the accession number GSE202603 (https://www.ncbi.nlm.nih.gov/geo/query/acc.cgi?acc=GSE202603).

Expanded View for this article is available online.

Acknowledgements
We thank Dr. Douglas A. Melton (Harvard University) for providing Pdx1-Cre mice and Dr. Shingo Usuki (Kumamoto University) for his technical support. We also thank the members of Dr. Yamagata's laboratory for their technical assistance and discussions. This study was supported by Grants-in-Aid for Scientific Research (B) from Japan Society for the Promotion of Science (JSPS) (19H03711 and 22H03129; KY), by a Grant-in-Aid for Challenging Research (Exploratory) from JSPS (19K22639; KY), and by a Grant-in-Aid for Scientific Research (C) from JSPS (19K09008; YS); by grants from the Takeda Science Foundation (KY and YS); and by grants from the program for Leading Graduate Schools HIGO (TT) and Center for Metabolic Regulation of Healthy Aging (TT) in Kumamoto university.

Author contributions
Tomonori Tsuyama: Conceptualization; data curation; formal analysis; funding acquisition; investigation; methodology; writing – original draft; writing – review and editing. **Yoshifumi Sato:** Conceptualization; data curation; formal analysis; supervision; funding acquisition; validation; investigation; methodology; writing – original draft; writing – review and editing. **Tatsuya Yoshizawa:** Conceptualization; supervision; writing – review

© 2023 The Authors

and editing. **Takaaki Matsuoka:** Conceptualization; resources; writing – review and editing. **Kazuya Yamagata:** Conceptualization; supervision; funding acquisition; writing – original draft; project administration; writing – review and editing.

Disclosure and competing interests statement

The authors declared that they have no conflict of interest.

References

Bensellam M, Duvillié B, Rybachuk G, Laybutt DR, Magnan C, Guiot Y, Pouysségur J, Jonas JC (2012) Glucose-induced O_2 consumption activates hypoxia inducible factors 1 and 2 in rat insulin-secreting pancreatic beta-cells. *PLoS One* 7: e29807

Bensellam M, Jonas JC, Laybutt DR (2018) Mechanisms of β-cell dedifferentiation in diabetes: recent findings and future research directions. *J Endocrinol* 236: R109 – R143

Cantley J, Selman C, Shukla D, Abramov AY, Forstreuter F, Esteban MA, Claret M, Lingard SJ, Clements M, Harten SK *et al* (2009) Deletion of the von Hippel-Lindau gene in pancreatic beta cells impairs glucose homeostasis in mice. *J Clin Invest* 119: 125 – 135

Cataldo LR, Singh T, Achanta K, Bsharat S, Prasad RB, Luan C, Renström E, Eliasson L, Artner I (2022) MAFA and MAFB regulate exocytosis-related genes in human β-cells. *Acta Physiol (Oxf)* 234: e13761

Catrina SB, Zheng X (2021) Hypoxia and hypoxia-inducible factors in diabetes and its complications. *Diabetologia* 64: 709 – 716

Cavadas MAS, Cheong A, Taylor CT (2017) The regulation of transcriptional repression in hypoxia. *Exp Cell Res* 356: 173 – 181

Chung SY, Kao CH, Villarroya F, Chang HY, Chang HC, Hsiao SP, Liou GG, Chen SL (2015) Bhlhe40 represses PGC-1α activity on metabolic gene promoters in myogenic cells. *Mol Cell Biol* 35: 2518 – 2529

Coppola T, Perret-Menoud V, Lüthi S, Farnsworth CC, Glomset JA, Regazzi R (1999) Disruption of Rab3-calmodulin interaction, but not other effector interactions, prevents Rab3 inhibition of exocytosis. *EMBO J* 18: 5885 – 5891

Dolai S, Xie L, Zhu D, Liang T, Qin T, Xie H, Kang Y, Chapman ER, Gaisano HY (2016) Synaptotagmin-7 functions to replenish insulin granules for exocytosis in human islet β-cells. *Diabetes* 65: 1962 – 1976

Fukui K, Yang Q, Cao Y, Takahashi N, Hatakeyama H, Wang H, Wada J, Zhang Y, Marselli L, Nammo T *et al* (2005) The HNF-1 target collectrin controls insulin exocytosis by SNARE complex formation. *Cell Metab* 2: 373 – 384

Gaston K, Jayaraman PS (2003) Transcriptional repression in eukaryotes: repressors and repression mechanisms. *Cell Mol Life Sci* 60: 721 – 741

Gerber PA, Rutter GA (2017) The role of oxidative stress and hypoxia in pancreatic Beta-cell dysfunction in diabetes mellitus. *Antioxid Redox Signal* 26: 501 – 518

Görlach A, Dimova EY, Petry A, Martínez-Ruiz A, Hernansanz-Agustín P, Rolo AP, Palmeira CM, Kietzmann T (2015) Reactive oxygen species, nutrition, hypoxia and diseases: problems solved? *Redox Biol* 6: 372 – 385

Gunton JE (2020) Hypoxia-inducible factors and diabetes. *J Clin Invest* 130: 5063 – 5073

Hang Y, Yamamoto T, Benninger RK, Brissova M, Guo M, Bush W, Piston DW, Powers AC, Magnuson M, Thurmond DC *et al* (2014) The MafA transcription factor becomes essential to islet β-cells soon after birth. *Diabetes* 63: 1994 – 2005

Huang W, Sherman BT, Lempicki RA (2009a) Bioinformatics enrichment tools: paths toward the comprehensive functional analysis of large gene lists. *Nucleic Acids Res* 37: 1 – 13

Huang W, Sherman BT, Lempicki RA (2009b) Systematic and integrative analysis of large gene lists using DAVID bioinformatics resources. *Nat Protoc* 4: 44 – 57

Hudish LI, Reusch JE, Sussel L (2019) β cell dysfunction during progression of metabolic syndrome to type 2 diabetes. *J Clin Invest* 129: 4001 – 4008

Ilegems E, Bryzgalova G, Correia J, Yesildag B, Berra E, Ruas JL, Pereira TS, Berggren PO (2022) HIF-1α inhibitor PX-478 preserves pancreatic β cell function in diabetes. *Sci Transl Med* 14: eaba9112

Ivanova A, Liao SY, Lerman MI, Ivanov S, Stanbridge EJ (2005) STRA13 expression and subcellular localisation in normal and tumour tissues: implications for use as a diagnostic and differentiation marker. *J Med Genet* 42: 565 – 576

Jarjour NN, Schwarzkopf EA, Bradstreet TR, Shchukina I, Lin CC, Huang SC, Lai CW, Cook ME, Taneja R, Stappenbeck TS *et al* (2019) Bhlhe40 mediates tissue-specific control of macrophage proliferation in homeostasis and type 2 immunity. *Nat Immunol* 20: 687 – 700

John AN, Ram R, Jiang FX (2018) RNA-seq analysis of islets to characterise the dedifferentiation in type 2 diabetes model mice db/db. *Endocr Pathol* 29: 207 – 221

Kahn SE, Cooper ME, Del Prato S (2014) Pathophysiology and treatment of type 2 diabetes: perspectives on the past, present, and future. *Lancet* 383: 1068 – 1083

Kelly DP, Scarpulla RC (2004) Transcriptional regulatory circuits controlling mitochondrial biogenesis and function. *Genes Dev* 18: 357 – 368

Kim D, Paggi JM, Park C, Bennett C, Salzberg SL (2019) Graph-based genome alignment and genotyping with HISAT2 and HISAT-genotype. *Nat Biotechnol* 37: 907 – 915

Kitamura T (2013) The role of FOXO1 in β-cell failure and type 2 diabetes mellitus. *Nat Rev Endocrinol* 9: 615 – 623

Ku HC, Cheng CF (2020) Master regulator activating transcription factor 3 (ATF3) in metabolic homeostasis and cancer. *Front Endocrinol (Lausanne)* 11: 556

LaGory EL, Wu C, Taniguchi CM, Ding CC, Chi JT, von Eyben R, Scott DA, Richardson AD, Giaccia AJ (2015) Suppression of PGC-1α is critical for reprogramming oxidative metabolism in renal cell carcinoma. *Cell Rep* 12: 116 – 127

Lee P, Chandel NS, Simon MC (2020) Cellular adaptation to hypoxia through hypoxia inducible factors and beyond. *Nat Rev Mol Cell Biol* 21: 268 – 283

Li D, Yin X, Zmuda EJ, Wolford CC, Dong X, White MF, Hai T (2008) The repression of IRS2 gene by ATF3, a stress-inducible gene, contributes to pancreatic beta-cell apoptosis. *Diabetes* 57: 635 – 644

Li H, Handsaker B, Wysoker A, Fennell T, Ruan J, Homer N, Marth G, Abecasis G, Durbin R (2009) The sequence alignment/map format and SAMtools. *Bioinformatics* 25: 2078 – 2079

Lin J, Handschin C, Spiegelman BM (2005) Metabolic control through the PGC-1 family of transcription coactivators. *Cell Metab* 1: 361 – 370

Ling C, Del Guerra S, Lupi R, Rönn T, Granhall C, Luthman H, Masiello P, Marchetti P, Groop L, Del Prato S (2008) Epigenetic regulation of PPARGC1A in human type 2 diabetic islets and effect on insulin secretion. *Diabetologia* 51: 615 – 622

Love MI, Huber W, Anders S (2014) Moderated estimation of fold change and dispersion for RNA-seq data with DESeq2. *Genome Biol* 15: 550

Mathelier A, Fornes O, Arenillas DJ, Chen CY, Denay G, Lee J, Shi W, Shyr C, Tan G, Worsley-Hunt R *et al* (2016) JASPAR 2016: a major expansion and update of the open-access database of transcription factor binding profiles. *Nucleic Acids Res* 44: D110 – D115

Miyazaki K, Kawamoto T, Tanimoto K, Nishiyama M, Honda H, Kato Y (2002) Identification of functional hypoxia response elements in the promoter region of the DEC1 and DEC2 genes. *J Biol Chem* 277: 47014 – 47021

 © 2023 The Authors

Nagamatsu S, Watanabe T, Nakamichi Y, Yamamura C, Tsuzuki K, Matsushima S (1999) Alpha-soluble N-ethylmaleimide-sensitive factor attachment protein is expressed in pancreatic beta cells and functions in insulin but not gamma-aminobutyric acid secretion. *J Biol Chem* 274: 8053 – 8060

Nishiyama Y, Goda N, Kanai M, Niwa D, Osanai K, Yamamoto Y, Senoo-Matsuda N, Johnson RS, Miura S, Kabe Y *et al* (2012) HIF-1α induction suppresses excessive lipid accumulation in alcoholic fatty liver in mice. *J Hepatol* 56: 441 – 447

Oh E, Kalwat MA, Kim MJ, Verhage M, Thurmond DC (2012) Munc18-1 regulates first-phase insulin release by promoting granule docking to multiple syntaxin isoforms. *J Biol Chem* 287: 25821 – 25833

Ohara-Imaizumi M, Fujiwara T, Nakamichi Y, Okamura T, Akimoto Y, Kawai J, Matsushima S, Kawakami H, Watanabe T, Akagawa K *et al* (2007) Imaging analysis reveals mechanistic differences between first- and second-phase insulin exocytosis. *J Cell Biol* 177: 695 – 705

Pertea M, Pertea GM, Antonescu CM, Chang TC, Mendell JT, Salzberg SL (2015) StringTie enables improved reconstruction of a transcriptome from RNA-seq reads. *Nat Biotechnol* 33: 290 – 295

Prentki M, Nolan CJ (2006) Islet beta cell failure in type 2 diabetes. *J Clin Invest* 116: 1802 – 1812

Puigserver P, Spiegelman BM (2003) Peroxisome proliferator-activated receptor-gamma coactivator 1 alpha (PGC-1 alpha): transcriptional coactivator and metabolic regulator. *Endocr Rev* 24: 78 – 90

Puri S, Cano DA, Hebrok M (2009) A role for von Hippel-Lindau protein in pancreatic beta-cell function. *Diabetes* 58: 433 – 441

Raum JC, Gerrish K, Artner I, Henderson E, Guo M, Sussel L, Schisler JC, Newgard CB, Stein R (2006) FoxA2, Nkx2.2, and PDX-1 regulate islet beta-cell-specific mafA expression through conserved sequences located between base pairs −8118 and −7750 upstream from the transcription start site. *Mol Cell Biol* 26: 5735 – 5743

Raum JC, Hunter CS, Artner I, Henderson E, Guo M, Elghazi L, Sosa-Pineda B, Ogihara T, Mirmira RG, Sussel L *et al* (2010) Islet beta-cell-specific MafA transcription requires the 5′-flanking conserved region 3 control domain. *Mol Cell Biol* 30: 4234 – 4244

Rorsman P, Renström E (2003) Insulin granule dynamics in pancreatic beta cells. *Diabetologia* 46: 1029 – 1045

Sato Y, Endo H, Okuyama H, Takeda T, Iwahashi H, Imagawa A, Yamagata K, Shimomura I, Inoue M (2011) Cellular hypoxia of pancreatic beta-cells due to high levels of oxygen consumption for insulin secretion in vitro. *J Biol Chem* 286: 12524 – 12532

Sato Y, Inoue M, Yoshizawa T, Yamagata K (2014) Moderate hypoxia induces β-cell dysfunction with HIF-1-independent gene expression changes. *PLoS One* 9: e114868

Sato F, Bhawal UK, Yoshimura T, Muragaki Y (2016) DEC1 and DEC2 crosstalk between circadian rhythm and tumor progression. *J Cancer* 7: 153 – 159

Sato Y, Tsuyama T, Sato C, Karim MF, Yoshizawa T, Inoue M, Yamagata K (2017) Hypoxia reduces HNF4α/MODY1 protein expression in pancreatic β-cells by activating AMP-activated protein kinase. *J Biol Chem* 292: 8716 – 8728

Scarpulla RC (2008) Transcriptional paradigms in mammalian mitochondrial biogenesis and function. *Physiol Rev* 88: 611 – 638

Shen L, Cui A, Xue Y, Cui Y, Dong X, Gao Y, Yang H, Fang F, Chang Y (2014) Hepatic differentiated embryo-chondrocyte-expressed gene 1 (Dec1) inhibits sterol regulatory element-binding protein-1c (Srebp-1c) expression and alleviates fatty liver phenotype. *J Biol Chem* 289: 23332 – 23342

Skarnes WC, Rosen B, West AP, Koutsourakis M, Bushell W, Iyer V, Mujica AO, Thomas M, Harrow J, Cox T *et al* (2011) A conditional knockout resource for the genome-wide study of mouse gene function. *Nature* 474: 337 – 342

St-Pierre B, Flock G, Zacksenhaus E, Egan SE (2002) Stra13 homodimers repress transcription through class B E-box elements. *J Biol Chem* 277: 46544 – 46551

Subramanian A, Tamayo P, Mootha VK, Mukherjee S, Ebert BL, Gillette MA, Paulovich A, Pomeroy SL, Golub TR, Lander ES *et al* (2005) Gene set enrichment analysis: a knowledge-based approach for interpreting genome-wide expression profiles. *Proc Natl Acad Sci U S A* 102: 15545 – 15550

Sun H, Taneja R (2000) Stra13 expression is associated with growth arrest and represses transcription through histone deacetylase (HDAC)-dependent and HDAC-independent mechanisms. *Proc Natl Acad Sci U S A* 97: 4058 – 4063

Turner RC, McCarthy ST, Holman RR, Harris E (1976) Beta-cell function improved by supplementing basal insulin secretion in mild diabetes. *Br Med J* 1: 1252 – 1254

Yamamoto K, Matsuoka TA, Kawashima S, Takebe S, Kubo F, Miyatsuka T, Kaneto H, Shimomura I (2013) A novel function of Onecut1 protein as a negative regulator of MafA gene expression. *J Biol Chem* 288: 21648 – 21658

Yun Z, Maecker HL, Johnson RS, Giaccia AJ (2002) Inhibition of PPAR gamma 2 gene expression by the HIF-1-regulated gene DEC1/Stra13: a mechanism for regulation of adipogenesis by hypoxia. *Dev Cell* 2: 331 – 341

Zehetner J, Danzer C, Collins S, Eckhardt K, Gerber PA, Ballschmieter P, Galvanovskis J, Shimomura K, Ashcroft FM, Thorens B *et al* (2008) pVHL is a regulator of glucose metabolism and insulin secretion in pancreatic β cells. *Genes Dev* 22: 3135 – 3146

Zhang C, Moriguchi T, Kajihara M, Esaki R, Harada A, Shimohata H, Oishi H, Hamada M, Morit N, Hasegawa K *et al* (2005) MafA is a key regulator of glucose-stimulated insulin secretion. *Mol Cell Biol* 25: 4969 – 4976

Zheng X, Zheng X, Wang X, Ma Z, Gupta Sunkari V, Botusan I, Takeda T, Björklund A, Inoue M, Catrina SB *et al* (2012) Acute hypoxia induces apoptosis of pancreatic β-cell by activation of the unfolded protein response and upregulation of CHOP. *Cell Death Dis* 3: e322

Zmuda EJ, Viapiano M, Grey ST, Hadley G, Garcia-Ocaña A, Hai T (2010a) Deficiency of Atf3, an adaptive-response gene, protects islets and ameliorates inflammation in a syngeneic mouse transplantation model. *Diabetologia* 53: 1438 – 1450

Zmuda EJ, Qi L, Zhu MX, Mirmira RG, Montminy MR, Hai T (2010b) The roles of ATF3, an adaptive-response gene, in high-fat-diet-induced diabetes and pancreatic beta-cell dysfunction. *Mol Endocrinol* 24: 1423 – 1433

© 2023 The Authors